Doctoral Dissertation

Studies on Novel Catalysts Based on SnO_2 or ZnO doped CeO_2-ZrO_2 for Complete Oxidation of Toluene

(酸化スズまたは酸化亜鉛が固溶したセリウムージルコニウム複合酸化物を用いた
新しいトルエン浄化触媒に関する研究)

Min Yeong Kim

January 2014

Department of Applied Chemistry
Graduate School of Engineering
Osaka University

Preface

The work of this thesis has been carried out under the supervision of Professor Dr. Nobuhito Imanaka at Department of Applied Chemistry, Graduate School of Engineering, Osaka University.

The object of this thesis is to develop novel catalysts based on SnO_2 or ZnO doped CeO_2-ZrO_2 for complete oxidation of toluene.

The author wishes that the findings of knowledge obtained in this study provide useful suggestions and information for further development and establishment of novel environmental catalysts and that the materials would contribute to more practical applications.

Min Yeong Kim

Department of Applied Chemistry
Graduate School of Engineering
Osaka University
2-1Yamadaoka, Suita, Osaka 565-0871
Japan

January 2014

Contents

General Introduction

Volatile organic compounds (VOCs) are organic chemical compounds such as aldehydes, ketones, and other light weight hydrocarbons. Since they have relatively high vapor pressures under ambient conditions, they vaporized easily and diffuse into the atmosphere. The VOCs are emitted in a variety of processes such as exhaust gases from the internal combustion engine, power generation plants, and chemical processing plants. Some VOCs are harmful to human health and the environment, and are recognized to cause sick building syndrome, multiple chemical sensitivity, and air pollution such as photo-chemical smog and ground-level ozone [1, 2].

Among the VOCs, toluene is widely used as an organic solvent for paints, printing inks, adhesives, and antiseptics due to its excellent ability to dissolve organic substances. However, toluene has an unpleasant odor and causes sick building syndrome by evaporating into the atmosphere. To protect our health and the environment from such noxious influences, it is necessary to remove toluene released into the atmosphere as much as possible.

For effective reduction, several methods have been proposed such as catalytic combustion [3], flame combustion [4], catalytic decomposition using ozone and plasma [5], photocatalytic decomposition [6], and the adsorbent-based method [7]. Among these methods, complete catalytic combustion of toluene into carbon dioxide and water vapor at moderate temperatures is an ecologically simple and clean technology to eliminate toluene [8]. A number of combustion catalysts for the elimination of toluene have been reported [9, 10].

Generally, catalysts for VOCs oxidation are classified into supported noble metals, metal oxides, and mixtures of noble metals and metal oxides [11-16]. The catalysis is affected by the influence of dispersed state of active compound and promoters, crystal structure, amount of active species, and surface area of the catalyst [15, 17]. Temperature is also an important parameter that affects the VOCs removal by oxidation catalysis. In addition, the properties of the toluene to be purified also play a key role in the selection of the catalyst and the determination of the reaction temperature [18].

Application of platinum supported catalysts is an effective way to eliminate toluene by complete oxidation. However, the conventional 5.0 wt%Pt/γ-Al_2O_3 catalyst was reported to be difficult to accomplish complete combustion of toluene at diverse environmental condition. Moreover, the catalyst needs to be heated to 170 °C at least [19, 20]. In particular, the use of platinum usually has high production costs, making it prohibitive from a practical application

standpoint. Therefore, it is desirable to develop catalysts devoid of platinum without a significant decrease in the catalytic activity. Furthermore, conventional Pt-supported catalysts usually deactivate after being exposed to high temperatures by the combustion heat over 1000 °C due to aggregation and growth of the platinum particles in spite of expensiveness of the metal [21-23]. Therefore, there is a real need for a novel oxidation catalyst with high-temperature endurance.

In several VOCs oxidation catalysts, CeO_2 and CeO_2-ZrO_2 solid solutions work effective promoters when they are in conjunction with platinum and metal oxides. In particular, some active platinum catalysts supported on them have been reported for VOCs oxidation [10, 24-30]. CeO_2 and CeO_2-ZrO_2 solid solutions can release and store oxygen corresponding to the surrounding atmosphere, and these properties make them attractive components as promoters of the automotive exhaust three-way catalysts [24].

In previous studies conducted by the research group, to which I belong it was found that employing such solid solutions, which have high oxygen release and storage properties, as promoters was effective to establish complete oxidation of VOCs at moderate temperatures [28-30]. In particular, introduction of a small amount of SnO_2, which has been well-known as a typical n-type semiconductor with electronic conduction [32], into the CeO_2-ZrO_2 lattice considerably facilitated the toluene oxidation [31], and my research group actually elucidated that Pt/CeO_2-ZrO_2-SnO_2/γ-Al_2O_3 catalysts had high VOCs oxidation activities at moderate temperatures [11-15]. However, a relatively large amount of platinum was supported on these catalysts, leading to high cost production from a practical application standpoint. Therefore, it is necessary to reduce the precious metal content in the catalysts as much as possible with no significant decrease in the catalytic activity. Furthermore, thermal stability of the toluene oxidation catalysis on the Pt/CeO_2-ZrO_2-SnO_2/γ-Al_2O_3 catalysts was not enough due to readily-reducibility of SnO_2.

In this study, therefore, reduction or free of platinum was aimed for each catalyst that can realize complete oxidation of toluene at a temperature as low as possible and that have high thermal stability even after being subjected to temperatures from over 1000 °C up to around 1400 °C.

This thesis consists of the following four chapters.

In Chapter 1, novel Pt/Co_3O_4/CeO_2-ZrO_2-SnO_2/γ-Al_2O_3 catalysts are described. Co_3O_4 and CeO_2-ZrO_2-SnO_2 solid solution were introduced to the conventional Pt/γ-Al_2O_3 catalyst to reduce the platinum content in the catalysts as much as possible with no significant decrease in the catalytic activity.

In Chapter 2, Co_3O_4/CeO_2-ZrO_2-SnO_2 catalysts are described. The component and composition of the catalysts described in Chapter 1 were carefully reviewed to realize catalysts free of platinum without a significant decrease in the catalytic activity.

In Chapter 3, development of Pt/CeO_2-ZrO_2-ZnO catalysts is described. In these catalysts, the platinum content was minimized to 0.4wt% and zinc oxide was applied as a substitute for SnO_2 in the promoter to increase the thermal stability of the catalyst support even after calcination at 1000 °C without significant decrease in the catalytic activity.

In Chapter 4, novel $La_{1-x}Ca_xCoO_{3-x/2}/CeO_2$-$ZrO_2$-ZnO catalysts are described. In the catalysts, the CeO_2-ZrO_2-ZnO solid solutions were used as the promoter, and $LaCoO_3$ and its solid solutions were employed as alternative materials for Pt to develop novel catalysts not only free of platinum but also have high thermal stability even after being subjected to temperatures from over 1000 °C up to around 1400 °C, because they show a gradual insulator–metal transition at moderate temperatures.

List of Publications

[1] Combustion of Toluene Catalyzed by $Pt/Co_3O_4/CeO_2$-ZrO_2-SnO_2/γ-Al_2O_3

Min Yeong Kim, Tomoya Kamata, Toshiyuki Masui, Nobuhito Imanaka

Journal of Materials Science Research, **2**, 51-59 (2013).

[2] Complete Oxidation of Toluene on Co_3O_4/CeO_2-ZrO_2-SnO_2 Catalysts

Min Yeong Kim, Tomoya Kamata, Toshiyuki Masui, Nobuhito Imanaka

Journal of Asian Ceramic Societies, **1**, 243-247 (2013).

[3] Complete Toluene Oxidation on Pt/CeO_2-ZrO_2-ZnO Catalysts

Min Yeong Kim, Tomoya Kamata, Toshiyuki Masui, Nobuhito Imanaka

Catalysts, **3**, 646-655 (2013).

[4] Complete Oxidation of Toluene on Refractory $La_{1-x}Ca_xCoO_{3-x/2}/CeO_2$-$ZrO_2$-ZnO Catalysts

Min Yeong Kim, Toshiyuki Masui, Nobuhito Imanaka

Catalysis Science & Technology, **4**, 321-324 (2014).

Chapter 1

Combustion of Toluene Catalyzed by $Pt/Co_3O_4/CeO_2$-ZrO_2-SnO_2/γ-Al_2O_3

1.1. Introduction

As mentioned in the General Introduction, a number of combustion catalysts for the reduction of toluene have been reported. However, it is difficult to accomplish complete combustion of toluene at low temperatures, because the catalysts usually need to be heated to at least 170 °C [9, 10, 19, 20].

In previous studies conducted by the research group, to which I belong it was found that a combination of platinum and a solid that can supply reactive oxygen molecules below 100 °C [34-38] was significantly effective in inducing the oxidation of VOCs by oxygen pullover from $Ce_{0.64}Zr_{0.16}Bi_{0.20}O_{1.90}/\gamma$-$Al_2O_3$ to platinum nanoparticles [28, 34]. In fact, my research group found that a 7wt%Pt/16wt%$Ce_{0.64}Zr_{0.16}Bi_{0.20}O_{1.90}/\gamma$-$Al_2O_3$ catalyst can completely oxidize toluene at 120 °C [29]. Furthermore, my research group demonstrated in our recent study that a 10wt%Pt/16wt%$Ce_{0.68}Zr_{0.17}Sn_{0.15}O_{2.00}/\gamma$-$Al_2O_3$ catalyst can completely oxidize toluene at a temperature as low as 110 °C [31]. However, a relatively large amount of platinum was supported on these catalysts, leading to high production cost from a practical application standpoint. Therefore, it is necessary to reduce the precious metal content in the catalysts as much as possible with no significant decrease in the catalytic activity.

To realize such advanced catalysts, I focused on cobalt oxide (Co_3O_4) as a promoter to facilitate the oxidation of toluene without excessive use of platinum, since Co_3O_4 was reported to have the highest catalytic activity for VOCs oxidation among several transition metal oxides investigated [40-45]. In this chapter, the amount of platinum was decreased to 1wt% and Co_3O_4 was employed as a promoter: 1wt%Pt/*x*wt%Co_3O_4/16wt%CeO_2-ZrO_2-SnO_2/γ-Al_2O_3 catalysts (x = 7, 11, and 15) were prepared and the effect of Co_3O_4 on the activity of toluene oxidation was investigated.

1.2. Experimental Procedure

A $Ce_{0.62}Zr_{0.20}Sn_{0.18}O_{2.00}/\gamma$-$Al_2O_3$ support was synthesized by co-precipitation and impregnation methods, the $Ce_{0.62}Zr_{0.20}Sn_{0.18}O_{2.00}$ was synthesized by co-precipitation and the

subsequent deposition on γ-Al_2O_3 was carried out by impregnation. SnC_2O_4 was dissolved in a mixture of 1.0 mol L^{-1} $Ce(NO_3)_3$ and 0.1 mol L^{-1} $ZrO(NO_3)_2$ aqueous solutions in a stoichiometric ratio, and then the mixture was impregnated on commercially available γ-Al_2O_3 (DK Fine, AA-300). The $Ce_{0.62}Zr_{0.20}Sn_{0.18}O_{2.00}$ content was adjusted to 16wt% of the total support to optimize the oxygen release ability [31]. The pH of the aqueous mixture was adjusted to 11 by dropwise addition of aqueous ammonia (5%), whereby the $Ce_{0.62}Zr_{0.20}Sn_{0.18}O_{2.00}$ particles were precipitated on the surface of γ-Al_2O_3. After stirring for 12 h at room temperature, the resulting $Ce_{0.62}Zr_{0.20}Sn_{0.18}O_{2.00}$/γ-$Al_2O_3$ support was collected by filtration, washed several times with deionized water, and then dried at 80 °C for 6 h. The sample was ground in an agate mortar and calcined at 600 °C for 1 h in an ambient atmosphere.

Supported cobalt oxide catalysts [*x*wt%Co_3O_4/16wt%$Ce_{0.62}Zr_{0.20}Sn_{0.18}O_{2.00}$/γ-$Al_2O_3$ (*x* = 7, 11, and 14)] were prepared by mixing a 0.1 mol L^{-1} $Co(NO_3)_3$ aqueous solution with the $Ce_{0.62}Zr_{0.20}Sn_{0.18}O_{2.00}$/γ-$Al_2O_3$ support. After mixing, the homogeneous samples were evaporated to dryness at 80 °C for 12 h, and then calcined at 500 °C for 1 h in an ambient atmosphere.

A supported platinum catalyst (1wt%Pt/*x*wt%Co_3O_4/16wt%$Ce_{0.62}Zr_{0.20}Sn_{0.18}O_{2.00}$/γ-$Al_2O_3$) was prepared by impregnating the *x*wt%Co_3O_4/16wt%$Ce_{0.62}Zr_{0.20}Sn_{0.18}O_{2.00}$/γ-$Al_2O_3$ support, in which the amount of Co_3O_4(*x*) was optimized to give the highest activity, with a 4wt% platinum colloid stabilized with polyvinylpyrrolidone in a water solvent (Tanaka Kikinzoku Kogyo Co., Ltd.). After impregnation, the sample was dried at 80 °C for 12 h, and then calcined at 450 °C or 500 °C for 4 h. For references, a 1wt%Pt/16wt%$Ce_{0.68}Zr_{0.17}Sn_{0.15}O_{2.00}$/γ-$Al_2O_3$ catalyst without Co_3O_4 and a 5wt%Pt/γ-Al_2O_3 catalyst were also prepared using the same procedure.

The sample compositions were analyzed using an X-ray fluorescence spectrometer (XRF; Rigaku, ZSX-100e). The crystal structures of the catalysts were identified by X-ray powder diffraction (XRD; Rigaku, SmartLab) using Cu-Kα radiation (40 kV, 30 mA). The Brunauer-Emmett-Teller (BET) specific surface area was measured by nitrogen adsorption at −196 °C and pore size distribution (PSD) plots were obtained by Barrett-Joyner-Halenda (BJH) method using the cylindrical pore model (Micromeritics Tristar 3000). X-ray photoelectron spectroscopy (XPS; ULVAC 5500MT) measurement was performed at room temperature using Mg-Kα radiation (1253.6 eV). The effect of charging on the binding energies was corrected with respect to the C 1s peak at 284.6 eV. Transmission electron microscopic images were also taken with an accelerating voltage of 200 kV (TEM; Hitachi H-800). Temperature programmed reduction (TPR) measurements were carried out under a flow of pure H_2 (80 mL min^{-1}) at a heating rate of 5 K min^{-1}

using a gas chromatograph with a thermal conductivity detector (TCD; Shimadzu GC-8AIT). Following the TPR experiments, the total oxygen storage capacity (OSC) was measured using a pulse-injection method at 427 °C (700 K).

The method for contacting the toluene with the catalyst can be different in catalytic oxidation systems. The oxidation activity for toluene was tested in a conventional fixed-bed flow reactor consisting of a 10-mm-diameter quartz glass tube. The feed gas was composed of 0.09 vol% toluene in an air balance and the rate was 20 mL min^{-1} over 0.1 g of the catalyst [space velocity (S.V.) = 12,000 L kg^{-1} h^{-1}]. Prior to the measurements, the catalyst was heated at 200 °C for 2 h in a flow of Ar (20 cm^3 min^{-1}) to remove water molecules adsorbed on the surface of the catalyst. The catalytic activity was evaluated in terms of toluene conversion. The gas composition after the reaction was analyzed using a gas chromatograph with a flame ionization detector (FID; Shimadzu GC-8AIF, Kyoto, Japan) in which the SunPak-A column was used for gas separation and a gas chromatograph-mass spectrometer (GC-Mass; Shimadzu GCMS-QP2010 Plus, Kyoto, Japan) in which the RTX624 column was installed.

1.3. Results and Discussion

Figure 1.1 shows XRD patterns of the 16wt%$Ce_{0.62}Zr_{0.20}Sn_{0.18}O_{2.00}$/γ-$Al_2O_3$ (CZS/Al_2O_3), 7wt%Co_3O_4/16wt%$Ce_{0.62}Zr_{0.20}Sn_{0.18}O_{2.00}$/γ-$Al_2O_3$ (7Co/CZS/Al_2O_3), 11wt%Co_3O_4/16wt%$Ce_{0.62}$-$Zr_{0.20}Sn_{0.18}O_{2.00}$/γ-$Al_2O_3$ (11Co/CZS/Al_2O_3), and 15wt%Co_3O_4/16wt%$Ce_{0.62}Zr_{0.20}Sn_{0.18}O_{2.00}$/γ-$Al_2O_3$ (15Co/CZS/Al_2O_3) catalysts. The XRD results for the CZS/Al_2O_3 support show only peaks corresponding to the cubic fluorite-type oxide, Co_3O_4, and γ-Al_2O_3, and no crystalline impurities were observed. The diffraction peaks assigned to the cubic fluorite type structure were steady and no peak shift was observed regardless of the amount of cobalt oxide, indicating that Co_3O_4 was supported on the surface of the CZS/Al_2O_3 support without forming solid solutions with CZS or γ-Al_2O_3.

BET specific surface areas of the CZS/Al_2O_3, 7Co/CZS/Al_2O_3, 11Co/CZS/Al_2O_3, and 15Co/CZS/Al_2O_3 catalysts are summarized in Table 1.1. The BET specific surface areas of the cobalt-supported catalysts were smaller than that of CZS/Al_2O_3, and they decreased with increasing Co_3O_4 content. These results suggest that some of the Co_3O_4 particles are supported in the pores of CZS/Al_2O_3.

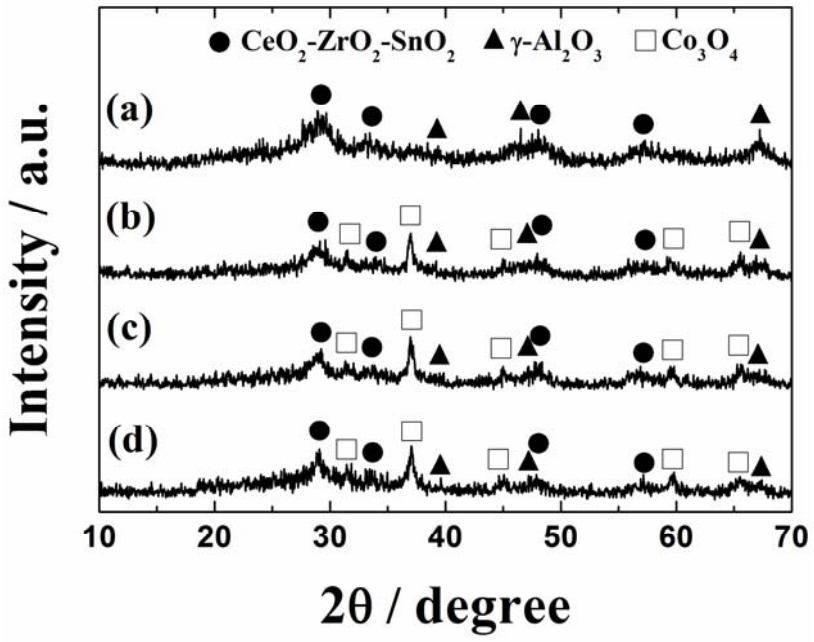

Figure 1.1 XRD patterns of the (a) 16wt%$Ce_{0.62}Zr_{0.20}Sn_{0.18}O_{2.00}$/γ-$Al_2O_3$, (b) 7wt%$Co_3O_4$/16wt%$Ce_{0.62}Zr_{0.20}Sn_{0.18}O_{2.00}$/γ-$Al_2O_3$, (c) 11wt%$Co_3O_4$/16wt%$Ce_{0.62}Zr_{0.20}Sn_{0.18}O_{2.00}$/γ-$Al_2O_3$, and (d) 15wt%$Co_3O_4$/16wt%$Ce_{0.62}Zr_{0.20}Sn_{0.18}O_{2.00}$/γ-$Al_2O_3$ catalysts (●:CeO_2-ZrO_2-SnO_2, ▲:γ-Al_2O_3, □:Co_3O_4).

Table 1.1 Composition and BET surface area of the catalysts

Catalyst	Catalyst composition	BET surface area ($m^2\ g^{-1}$)
CZS/Al_2O_3	16wt%$Ce_{0.62}Zr_{0.20}Sn_{0.18}O_{2.00}$/γ-$Al_2O_3$	190
7Co/CZS/Al_2O_3	7wt%Co_3O_4/16wt%$Ce_{0.62}Zr_{0.20}Sn_{0.18}O_{2.00}$/γ-$Al_2O_3$	151
11Co/CZS/Al_2O_3	11wt%Co_3O_4/16wt%$Ce_{0.62}Zr_{0.20}Sn_{0.18}O_{2.00}$/γ-$Al_2O_3$	141
15Co/CZS/Al_2O_3	15wt%Co_3O_4/16wt%$Ce_{0.62}Zr_{0.20}Sn_{0.18}O_{2.00}$/γ-$Al_2O_3$	139
1Pt/11Co/Al_2O_3	1wt%Pt/11wt%Co_3O_4/γ-Al_2O_3	166
1Pt/CZS/Al_2O_3	1wt%Pt/16wt%$Ce_{0.62}Zr_{0.20}Sn_{0.18}O_{2.00}$/γ-$Al_2O_3$	176
1Pt/11Co/CZS/Al_2O_3	1wt%Pt/11wt%Co_3O_4/16wt%$Ce_{0.62}Zr_{0.20}Sn_{0.18}O_{2.00}$/γ-$Al_2O_3$	131

Figure 1.2 depicts temperature dependencies of toluene oxidation over the 7Co/CZS/Al_2O_3, 11Co/CZS/Al_2O_3, and 15Co/CZS/Al_2O_3 catalysts. Toluene was completely oxidized into CO_2 and water vapor, and no CO and toluene-derived compounds were detected as by-products with a gas

chromatograph. The toluene oxidation activity depends on the catalyst composition, and the highest activity was obtained for 11Co/CZS/Al_2O_3. However, the activity decreased with increasing Co_3O_4 content beyond the optimum amount, probably due to Co_3O_4 agglomeration and particle growth. Toluene oxidation activity of the optimum 11Co/CZS/Al_2O_3 catalyst was initially observed at 100 °C, and complete oxidation of toluene was confirmed at 300 °C. Unfortunately, this temperature was higher than that of 10wt%Pt/16wt%$Ce_{0.68}Zr_{0.17}Sn_{0.15}O_{2.00}$/γ-$Al_2O_3$ (110 °C) previously reported by our group [31]. Therefore, to increase the catalytic activity of 11Co/CZS/Al_2O_3, a small amount of platinum (1wt%) was additionally supported on the surface of the catalyst.

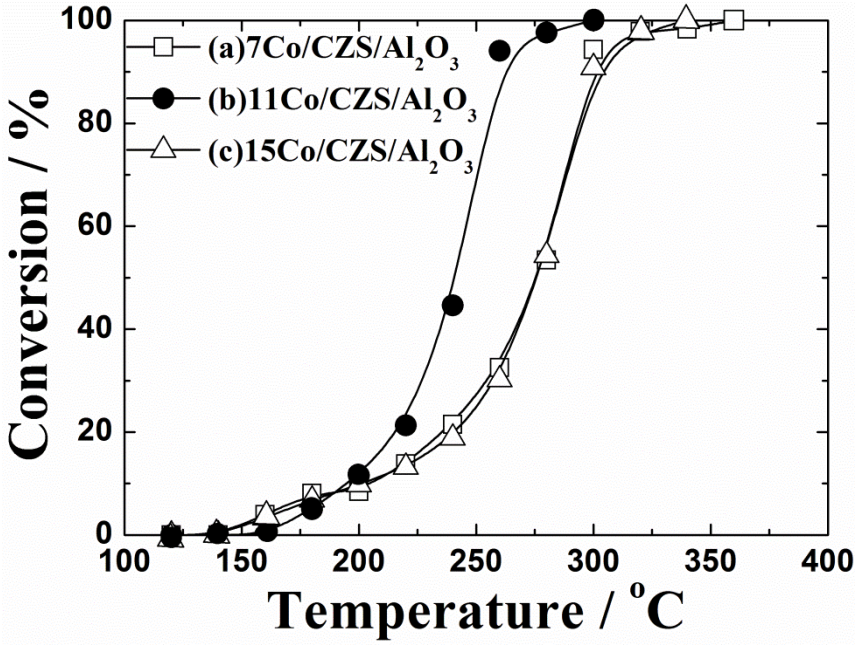

Figure 1.2 Temperature dependencies of toluene oxidation on the (a) 7wt%Co_3O_4/16wt%$Ce_{0.62}Zr_{0.20}Sn_{0.18}O_{2.00}$/γ-$Al_2O_3$, (b) 11wt%$Co_3O_4$/16wt%$Ce_{0.62}Zr_{0.20}Sn_{0.18}O_{2.00}$/γ-$Al_2O_3$, and (c) 15wt% Co_3O_4/16wt%$Ce_{0.62}Zr_{0.20}Sn_{0.18}O_{2.00}$/γ-$Al_2O_3$ catalysts.

Figure 1.3 shows XRD patterns of 1wt%Pt/11wt%Co_3O_4/16wt%$Ce_{0.62}Zr_{0.20}Sn_{0.18}O_{2.00}$/γ-$Al_2O_3$ (1Pt/11Co/CZS/Al_2O_3) and 1wt%Pt/16wt%$Ce_{0.62}Zr_{0.20}Sn_{0.18}O_{2.00}$/γ-$Al_2O_3$ (1Pt/CZS/Al_2O_3). In addition, in these cases, only $Ce_{0.62}Zr_{0.20}Sn_{0.18}O_{2.00}$, Co_3O_4, and γ-Al_2O_3 were observed in the XRD patterns and no peaks corresponding to platinum appeared probably due to the small platinum particles that are highly dispersed on the surface of the catalysts.

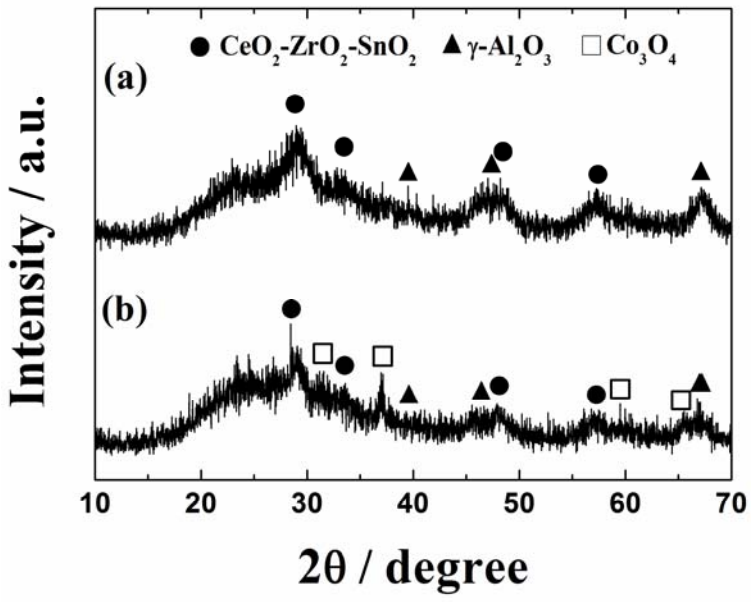

Figure 1.3 XRD patterns of the (a) 1wt%Pt/16wt%$Ce_{0.62}Zr_{0.20}Sn_{0.18}O_{2.00}$/γ-$Al_2O_3$ and (b) 1wt%Pt/ 11wt%Co_3O_4/16wt%$Ce_{0.62}Zr_{0.20}Sn_{0.18}O_{2.00}$/γ-$Al_2O_3$ catalysts (●:CeO_2-ZrO_2-SnO_2, ▲:γ-Al_2O_3, □:Co_3O_4).

The bright and dark field TEM images of 1Pt/11Co/CZS/Al_2O_3 and 1Pt/CZS/Al_2O_3 are depicted in Figure 1.4. As shown by these photographs, there is no clear difference in the size and dispersion state of platinum particles in these catalysts, which are recognized as bright spots in the dark field images in Figures 1.4(b) and (d). The particle size of platinum was estimated using these spots and it was confirmed to be smaller than 5 nm for both catalysts. Furthermore, it is also found that Co_3O_4 is presented as needle crystals by comparing the bright field image of 1Pt/11Co/CZS/Al_2O_3 with that of 1Pt/CZS/Al_2O_3. BET specific surface areas of 1Pt/CZS/Al_2O_3 and 1Pt/11Co/CZS/Al_2O_3 are also listed in Table 1.1. The surface area of the latter is smaller than that of the former, which might be as a result of the Co_3O_4 deposition in the pore of CZS/Al_2O_3, as mentioned above.

The BJH desorption pore size distribution plots of 1Pt/CZS/Al_2O_3 and 1Pt/11Co/CZS/Al_2O_3 are shown in Figure 1.5. As evidenced in this figure, these catalyst particles have a narrow mesopore size distribution at 6 nm and the size was maintained even if Co_3O_4 was deposited on $Ce_{0.62}Zr_{0.20}Sn_{0.18}O_{2.00}$/γ-$Al_2O_3$. However, the pore volume was significantly decreased by the Co_3O_4 deposition, which supports the above discussion.

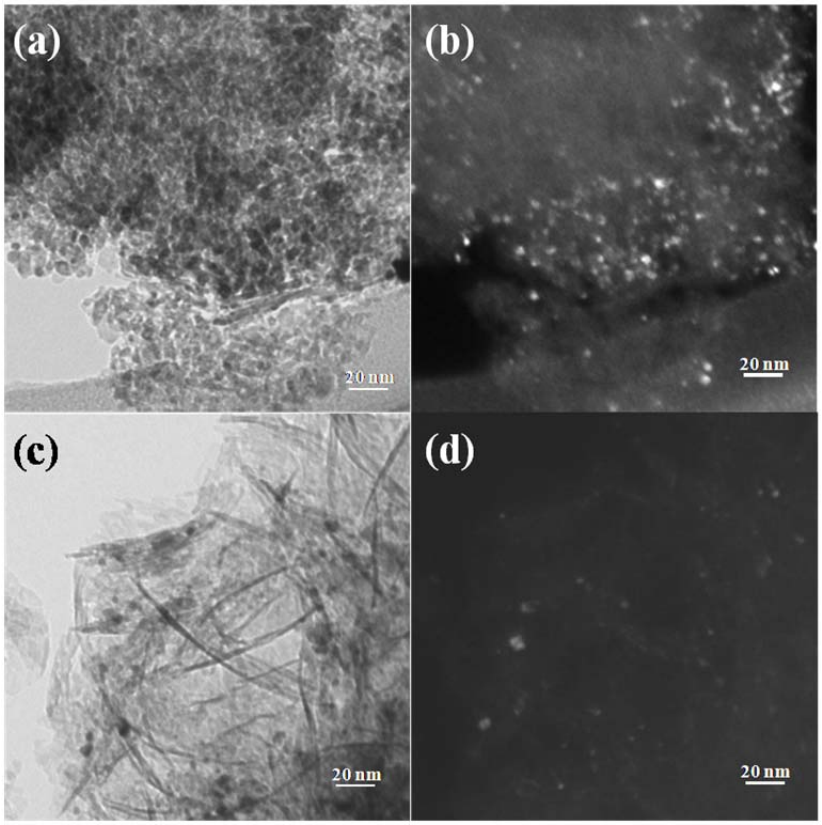

Figure 1.4 Transmission electron micrographs (TEM) of the (a), (b) 1wt%Pt/16wt%$Ce_{0.62}Zr_{0.20}$-$Sn_{0.18}O_{2.00}$/γ-Al_2O_3, and (c), (d) 1wt%Pt/11wt%Co_3O_4/16wt%$Ce_{0.62}Zr_{0.20}Sn_{0.18}O_{2.00}$/γ-$Al_2O_3$ catalysts : (a), (c) are bright field images, and (b), (d) are dark field images.

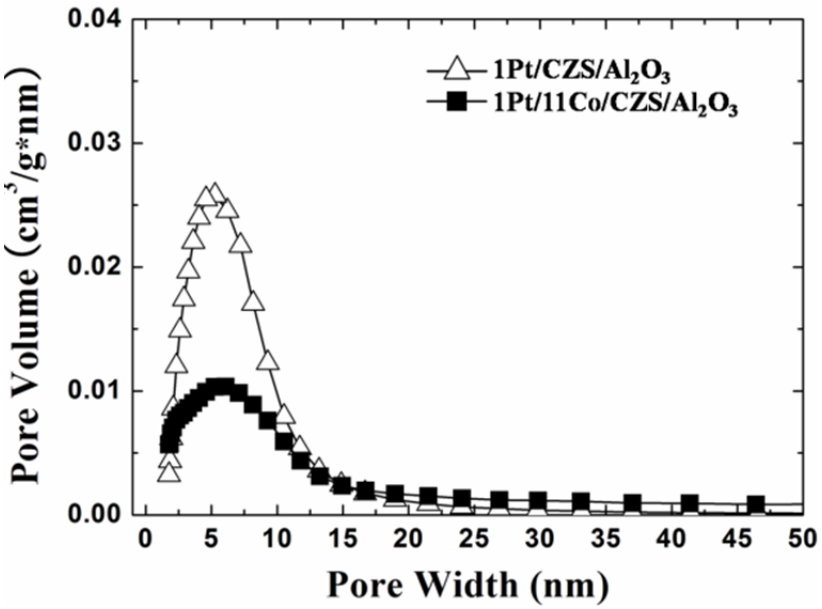

Figure 1.5 BJH pore distribution plots of the 1wt%Pt/16wt%$Ce_{0.62}Zr_{0.20}Sn_{0.18}O_{2.00}$/γ-$Al_2O_3$ and 1wt%Pt/11wt%Co_3O_4/16wt%$Ce_{0.62}Zr_{0.20}Sn_{0.18}O_{2.00}$/γ-$Al_2O_3$ catalysts.

Figure 1.6 shows the temperature dependencies of toluene oxidation over the 1Pt/11Co/CZS/Al_2O_3 and 11Co/CZS/Al_2O_3 catalysts. Results for 1Pt/CZS/Al_2O_3, 1Pt/11Co/Al_2O_3, and conventional 5wt%Pt/γ-Al_2O_3 are also plotted for comparison. The total oxidation of toluene to CO_2 and water vapor was confirmed for all catalysts. The toluene oxidation activity of 11Co/CZS/Al_2O_3 was significantly enhanced by the addition of platinum, and despite a smaller platinum loading in the present catalysts, toluene was completely oxidized at a lower temperature of 160 °C compared to that using 5wt%Pt/γ-Al_2O_3 (170 °C). Furthermore, the present 1Pt/11Co/CZS/Al_2O_3 catalyst (complete oxidation of toluene at 160 °C) is more active than 1Pt/CZS/Al_2O_3 (180 °C), indicating the advantage of Co_3O_4 addition to CZS/Al_2O_3. However, the presence of CZS is indispensable because the oxidation activity of 1Pt/11Co/Al_2O_3 (210 °C) is smaller than that of 1Pt/11Co/CZS/Al_2O_3 (160 °C).

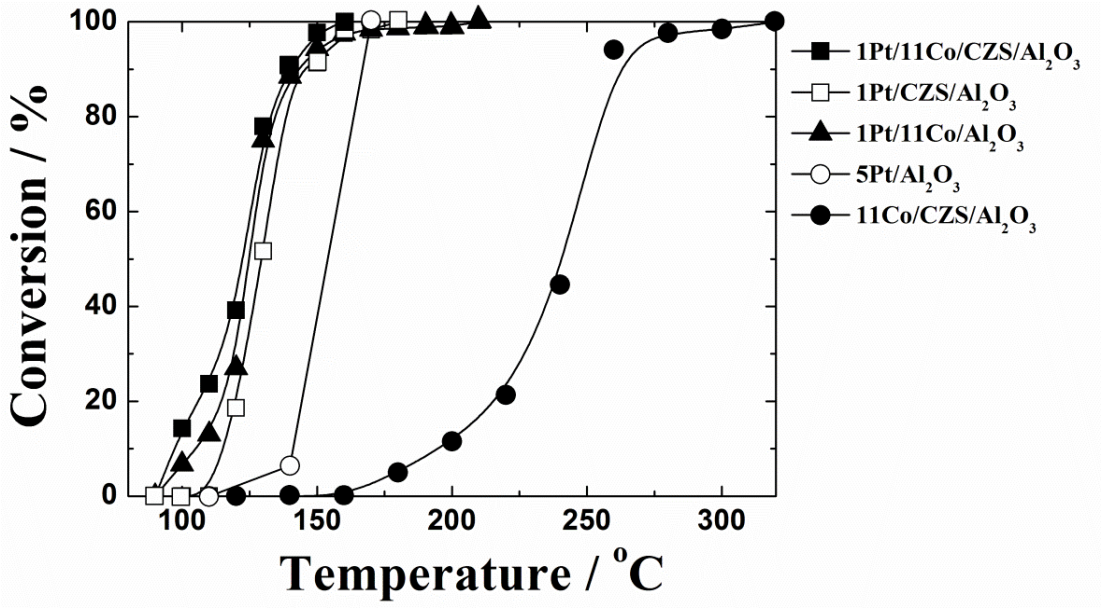

Figure 1.6 Temperature dependencies of toluene oxidation on the 1wt%Pt/11wt%Co_3O_4/16wt%$Ce_{0.62}Zr_{0.20}Sn_{0.18}O_{2.00}$/γ-$Al_2O_3$ (■), 11wt%Co_3O_4/16wt%$Ce_{0.62}Zr_{0.20}Sn_{0.18}O_{2.00}$/γ-$Al_2O_3$ (●), 1wt%Pt/16wt%$Ce_{0.62}Zr_{0.20}Sn_{0.18}O_{2.00}$/γ-$Al_2O_3$ (▲), 1wt%Pt/11wt%Co_3O_4/γ-Al_2O_3 (□), and 5wt%Pt/γ-Al_2O_3 (○) catalysts.

In addition, a supported platinum catalyst was also prepared at 450 °C. The temperature dependencies of toluene oxidation on the 1wt%Pt/11wt%Co_3O_4/16wt%$Ce_{0.62}Zr_{0.20}Sn_{0.18}O_{2.00}$/γ-$Al_2O_3$ catalysts calcined at 450 and 500 °C is shown in Figure 1.7. Unfortunately, the oxidation activity was not improved. Therefore, the calcination temperature of 500 °C is appropriate for the

supported platinum catalyst.

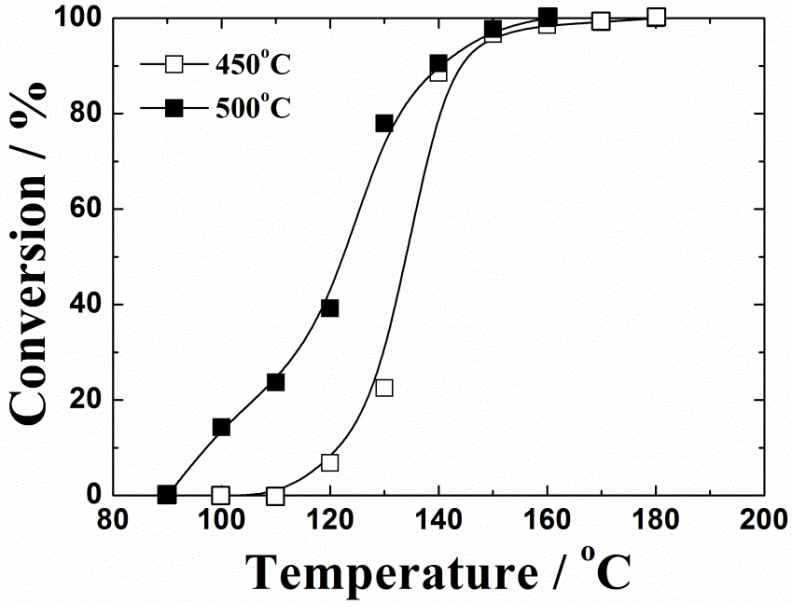

Figure 1.7 Temperature dependencies of toluene oxidation on the 1wt%Pt/11wt%Co_3O_4/ 16wt%$Ce_{0.62}Zr_{0.20}Sn_{0.18}O_{2.00}$/γ-$Al_2O_3$ catalysts calcined at 450 °C (□) and 500 °C (■).

To identify the cause for the positive effect of Co_3O_4, TPR spectra of 11Co/CZS/Al_2O_3 and CZS/Al_2O_3 are measured and their oxygen release behaviors were compared as shown in Figure 1.8. In the case of CZS/Al_2O_3, the oxygen release peak was observed at 92 °C, while the peak appeared at a lower temperature of 78 °C for 11Co/CZS/Al_2O_3. Accordingly, the introduction of Co_3O_4 on the CZS/Al_2O_3 support was remarkably effective in enhancing the oxygen supply capability at low temperatures. Furthermore, the total oxygen storage capacity of 11Co/CZS/Al_2O_3 was 388 μmol O_2 g^{-1}, which was 2.5 times larger than that of CZS/Al_2O_3 (140 μmol O_2 g^{-1}). The increase in the oxygen release and storage abilities was due to the synergistic effects of three redox couples of Ce^{4+}/Ce^{3+}, Sn^{4+}/Sn^{2+}, and Co^{3+}/Co^{2+}, whereby the toluene oxidation was facilitated. As a result, the introduction of Co_3O_4 as a promoter was highly effective in enhancing the catalytic activity.

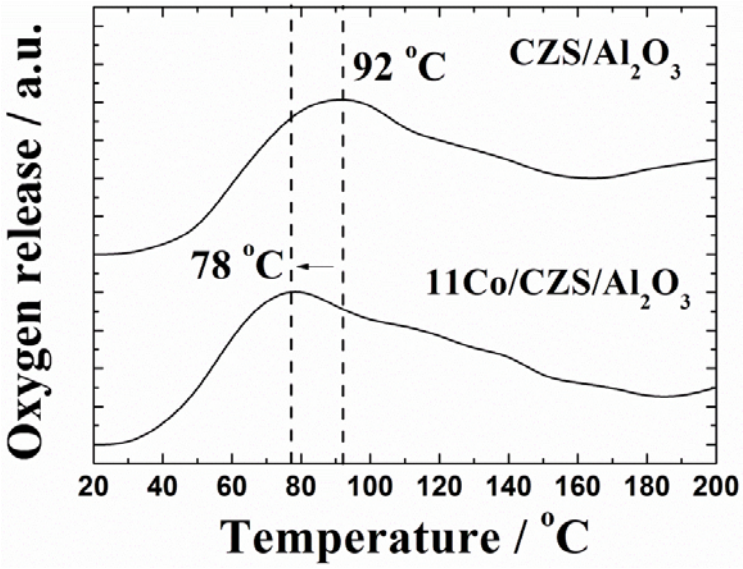

Figure 1.8 TPR profiles of the 16wt%$Ce_{0.62}Zr_{0.20}Sn_{0.18}O_{2.00}$/γ-$Al_2O_3$ and 11wt%Co_3O_4/16wt% $Ce_{0.62}Zr_{0.20}Sn_{0.18}O_{2.00}$/γ-$Al_2O_3$ catalysts.

The oxidation states of Ce, Sn, Co, and Pt in the 1Pt/11Co/CZS/Al_2O_3 catalyst were analyzed by XPS. The XPS results of Ce 3d, Sn 3d, Co 2p, and Pt 4f core-levels are shown in Figure 1.9. From Figures 1.9(a) and (b), it is evident that cerium exists both in the trivalent and tetravalent states [47, 48], while tin remains in the tetravalent state and no peaks of the Sn^{2+} species are observed [31, 49]. In the case of cobalt, the Co 2p peaks in Figure 1.9(c) are deconvoluted into five peaks. The Co $2p_{3/2}$ and $2p_{3/2}$ peaks can be attributed to the divalent (Co^{2+}: 780.8 and 796.3 eV) and trivalent (Co^{3+}: 779.5 and 794.5 eV) oxidation states, and the broad one at 786.0 eV corresponds to a satellite peak of Co^{2+} [46, 50]. These are the typical results for Co_3O_4 [44]. The Pt 4f peaks are shown in Figure 1.9(d). Although the Pt $4f_{5/2}$ peak at 74.4 eV overlaps that of Al 2p in the present case, the small Pt $4f_{7/2}$ peak is clearly observed at 70.9 eV, which can be attributed to the metallic platinum (Pt^0) [51].

Taking into account of the catalysis, TPR, and XPS results, the high oxidation activity of toluene observed in 1Pt/11Co/CZS/Al_2O_3 can be attributed to a concerted effect of Pt, Co_3O_4, and $Ce_{0.62}Zr_{0.20}Sn_{0.18}O_{2.00}$ supported on γ-Al_2O_3. The readily reducible Co_3O_4 and $Ce_{0.62}Zr_{0.20}Sn_{0.18}O_{2.00}$ contribute to the supplementation of active oxygen species from the catalyst bulk, and the oxygen reacts with toluene at the interface of three Pt, Co_3O_4, and $Ce_{0.62}Zr_{0.20}Sn_{0.18}O_{2.00}$ phases. As a result, complete toluene oxidation was realized using the present 1Pt/11Co/CZS/Al_2O_3 catalyst at a temperature of 160 °C which is lower than that of 5wt%Pt/γ-Al_2O_3 (170 °C), in spite of a smaller amount of platinum.

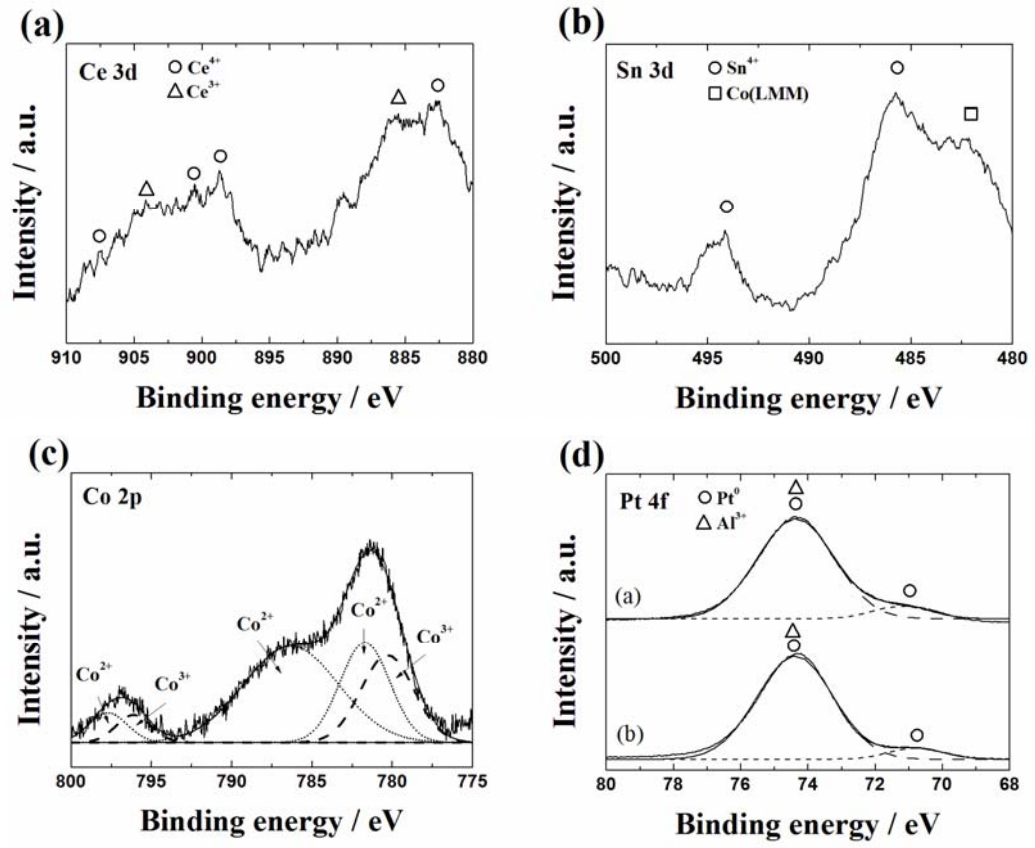

Figure 1.10 XPS results of the 1wt%Pt/11wt%Co_3O_4/16wt%$Ce_{0.62}Zr_{0.20}Sn_{0.18}O_{2.00}$/γ-$Al_2O_3$ catalyst : (a) Ce 3d, (b) Sn 3d, (c) Co 2p, and (d) Pt 4f core-levels.

1.4. Conclusions

Novel Co_3O_4/CeO_2-ZrO_2-SnO_2/γ-Al_2O_3 and Pt/Co_3O_4/CeO_2-ZrO_2-SnO_2/γ-Al_2O_3 catalysts were successfully prepared by the conventional co-precipitation and impregnation methods. The catalytic tests for toluene oxidation on these materials showed that addition of Co_3O_4 to a Pt/CeO_2-ZrO_2-SnO_2/γ-Al_2O_3 catalyst was significantly effective in decreasing the amount of platinum without significant reduction in the activity. In fact, complete oxidation of toluene was realized using the 1wt%Pt/11wt%Co_3O_4/16wt%$Ce_{0.62}Zr_{0.20}Sn_{0.18}O_{2.00}$/γ-$Al_2O_3$ catalyst at 160 °C, which was lower than that using the 5wt%Pt/γ-Al_2O_3 catalyst (170 °C). Since the oxidation activities of 1wt%Pt/16wt%$Ce_{0.62}Zr_{0.20}Sn_{0.18}O_{2.00}$/γ-$Al_2O_3$ and 1wt%Pt/11wt%Co_3O_4/γ-Al_2O_3 were lower than that of 1wt%Pt/11wt%Co_3O_4/16wt%$Ce_{0.62}Zr_{0.20}Sn_{0.18}O_{2.00}$/γ-$Al_2O_3$, the cause for the high toluene oxidation activity observed in the 1wt%Pt/11wt%Co_3O_4/16wt%$Ce_{0.62}Zr_{0.20}Sn_{0.18}O_{2.00}$ /γ-Al_2O_3 catalyst can be attributed to the concerted effect of Pt, Co_3O_4, and $Ce_{0.62}Zr_{0.20}Sn_{0.18}O_{2.00}$ supported on γ-Al_2O_3.

Chapter 2

Complete Oxidation of Toluene on Co_3O_4/CeO_2-ZrO_2-SnO_2 Catalysts

2.1. Introduction

In Chapter 1, it was demonstrated that the $Pt/Co_3O_4/CeO_2$-ZrO_2-SnO_2/γ-Al_2O_3 catalysts are significantly active for oxidation of toluene. Furthermore, this catalyst reduced the amount of Pt down to 1/5, compared to the conventional 5wt%Pt/γ-Al_2O_3 catalyst. Since the high oxidation activities for toluene are attributed to the combination of the excellent oxygen release property of CeO_2-ZrO_2-SnO_2 and high oxidation activity for the concerted effect of Co_3O_4 and Pt.

Application of platinum supported catalysts is an effective way to eliminate toluene by complete oxidation. However, the use of platinum usually has high production costs, making it prohibitive from a practical application standpoint. Therefore, it is desirable to develop catalysts devoid of platinum without a significant decrease in the catalytic activity.

To realize such advanced catalysts, I focused on cobalt oxide (Co_3O_4) instead of platinum as a catalyst to facilitate toluene oxidation, since Co_3O_4 was reported to have the highest catalytic activity for VOCs oxidation among several transition metal oxides investigated [41-46]. Furthermore, the use of catalyst supports, which can provide oxygen from inside the bulk, is also effective in facilitating toluene oxidation [10].

Therefore, the high oxidation activities for toluene described in Chapter 1 were successfully realized by the cause for the high toluene oxidation activity observed in the 1wt%Pt/11wt%Co_3O_4/16wt%$Ce_{0.62}Zr_{0.20}Sn_{0.18}O_{2.00}/\gamma$-$Al_2O_3$ catalyst, according to the concerted effect of Co_3O_4 and $Ce_{0.62}Zr_{0.20}Sn_{0.18}O_{2.00}$. This improvement of the oxygen release ability of the catalyst can be ascribed to the simultaneous reduction of Ce^{4+} and Sn^{4+} in the CeO_2-ZrO_2-SnO_2 solid solutions. Co_3O_4 on the CeO_2-ZrO_2-SnO_2 supports promoted toluene oxidation in lieu of platinum, which is usually employed but leads to high production costs. Therefore, interaction of CeO_2-ZrO_2-SnO_2 and Co_3O_4 are expected to promote the complete oxidation of toluene.

Employing the CeO_2-ZrO_2-SnO_2 solid solutions was even more effective in accelerating toluene oxidation [31]. In this study, therefore, the novel Co_3O_4/CeO_2-ZrO_2-SnO_2 catalysts were prepared and catalytic combustion of toluene on the catalysts was investigated to realize complete abatement of toluene at as low a temperature as possible.

In **Chapter 2**, novel Co_3O_4/CeO_2-ZrO_2-SnO_2 catalysts, in which the cobalt oxide is supported on the high oxygen storage capacity CeO_2-ZrO_2-SnO_2 support, are described. The oxidation activities for toluene were investigated.

2.2. Experimental Procedure

A $Ce_{0.67}Zr_{0.18}Sn_{0.15}O_{2.00}$ support was prepared by the evaporative drying method, where the composition was optimized to give the highest oxygen release and storage abilities [31]. SnC_2O_4 was dissolved in a mixture of 1.0 mol dm^{-3} $Ce(NO_3)_3$ and 0.1 mol dm^{-3} $ZrO(NO_3)_2$ aqueous solutions in a stoichiometric ratio. Next, citric acid, acetic acid (30 w/v%), and polyvinyl pyrrolidone K25 (PVP; mean molecular weight of 35,000 and mean degree of polymerization of 315) were added and the solution was stirred at 80 °C for 6 h. After the solvent was evaporated at 180 °C on an agitator with a heater, the resulting powder was dried at 80 °C for 12 h, and then calcined at 500 °C for 1 h.

Supported $x$wt%$Co_3O_4/Ce_{0.67}Zr_{0.18}Sn_{0.15}O_{2.00}$ ($10 \leq x \leq 20$) catalysts were prepared by mixing a 0.1 mol dm^{-3} $Co(NO_3)_3$ aqueous solution with the $Ce_{0.67}Zr_{0.18}Sn_{0.15}O_{2.00}$ support. After mixing, homogeneous samples were obtained by evaporative drying at 80 °C for 12 h, and then calcination at 500 °C for 4 h to generate the spinel structure of Co_3O_4 certainly. For reference, a catalyst without SnO_2 using the same procedure was prepared. In addition, a 16.8wt%$Co_3O_4/Ce_{0.78}Zr_{0.22}O_{2.00}$ catalyst and a 16.8wt%$Co_3O_4/Ce_{0.64}Zr_{0.15}Bi_{0.21}O_{1.895}$ catalyst were prepared by a similar procedure for comparison.

The sample composition was analyzed by X-ray fluorescence spectrometry (XRF; Rigaku, ZSX-100e). The crystal structure of the catalysts was identified by X-ray powder diffraction (XRD; Rigaku, SmartLab) using Cu-Kα radiation (40 kV, 30 mA). Transmission electron microscopic images were also taken, operating with an accelerating voltage of 300 kV (TEM; Hitachi H-9000NAR). The Brunauer-Emmett-Teller (BET) specific surface area was measured by nitrogen adsorption at −196 °C and pore size distribution (PSD) plots were obtained by the Barrett-Joyner-Halenda (BJH) method using the cylindrical pore model (Micromeritics Tristar 3000). Temperature programmed reduction (TPR) measurements were carried out under a flow of 5 vol% H_2-Ar (50 cm^3 min^{-1}) at a heating rate of 5 °C min^{-1} (BEL JAPAN BELCAT-B). Following the TPR experiment, the oxygen storage capacity (OSC) was measured using a pulse-injection method at 427 °C (700 K).

The oxidation activity for toluene was tested by the similar procedure described in Chapter 1. The feed gas was composed of 0.09 vol% toluene in an air balance and the rate was 20 cm^3 min^{-1} over 0.1 g of the catalyst, where the space velocity is 12,000 dm^3 kg^{-1} h^{-1}.

2.3. Results and Discussion

Figure 2.1 shows in the XRD patterns of $Ce_{0.78}Zr_{0.22}O_{2.00}$ (CZ), $Ce_{0.64}Zr_{0.15}Bi_{0.21}O_{1.895}$ (CZB) and $Ce_{0.67}Zr_{0.18}Sn_{0.15}O_{2.00}$ (CZS) supports. As seen in the enlargement of the patterns in the 2θ range from 55 to 58°, the XRD peaks of CZB shifted to lower angles, while the peaks of CZS shifted to higher angles than those of CZ, respectively, because Bi^{3+} (ionic radius: 0.117 nm) [52] is larger and Sn^{4+} (ionic radius: 0.081 nm) [52] is smaller than Ce^{4+} (ionic radius: 0.097 nm) [52] and Zr^{4+} (ionic radius: 0.084 nm) [52] in the host lattice. The cubic lattice constants were 0.5381 nm for CZ, 0.5405 nm for CZB, and 0.5354 nm for CZS, respectively, which were calculated from the XRD peak angles, refined using α-Al_2O_3 as a standard. These lattice expansion and shrink elucidate the formation of solid solutions.

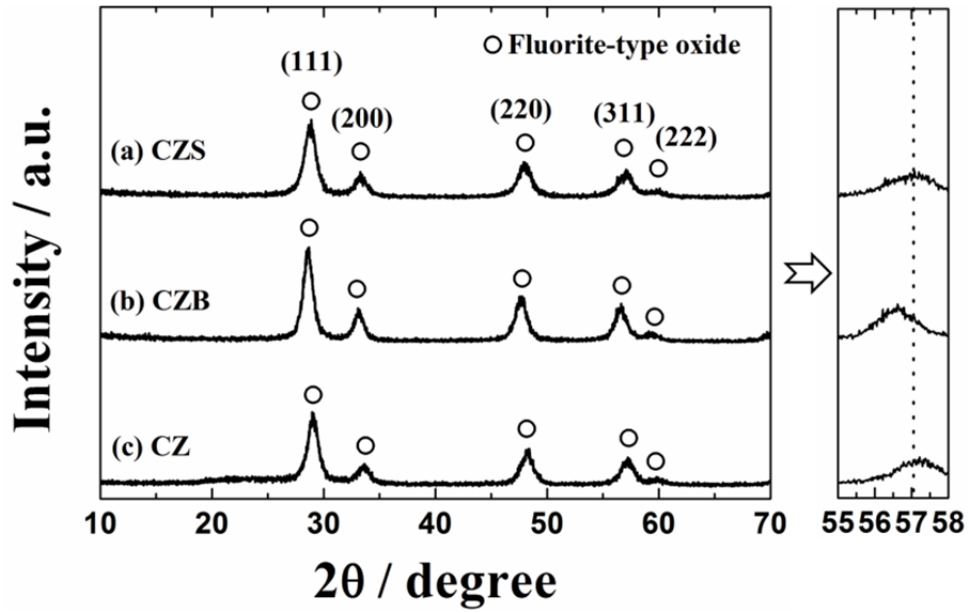

Figure 2.1. XRD patterns for (a) $Ce_{0.67}Zr_{0.18}Sn_{0.15}O_{2.0}$ (CZS), (b) $Ce_{0.64}Zr_{0.15}Bi_{0.21}O_{1.895}$ (CZB), and (c) $Ce_{0.78}Zr_{0.22}O_{2.0}$ (CZ).

Figure 2.2 shows XRD patterns for the *x*wt%Co_3O_4/$Ce_{0.67}Zr_{0.18}Sn_{0.15}O_{2.00}$ ($10 \leq x \leq 20$) catalysts. The XRD results for the *x*wt%Co_3O_4/$Ce_{0.67}Zr_{0.18}Sn_{0.15}O_{2.0}$ (*x*Co/CZS) catalysts showed only peaks corresponding to the cubic fluorite-type oxide (CeO_2; JCPDS 34-0394), Co_3O_4 (JCPDS 42-1467), and no crystalline impurities were observed. No peak shift was observed regardless of the amount of cobalt oxide, indicating that Co_3O_4 was supported on the surface of the $Ce_{0.67}Zr_{0.18}Sn_{0.15}O_{2.00}$ without forming solid solutions.

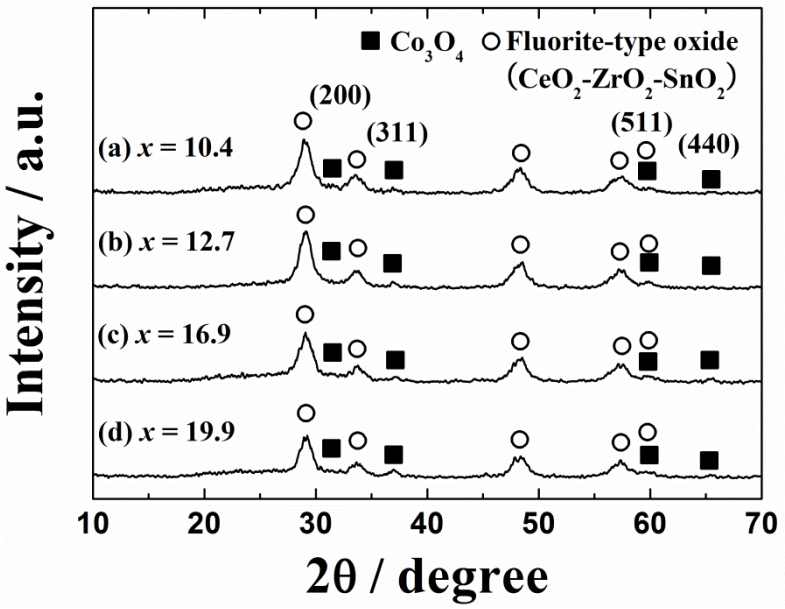

Figure 2.2. XRD patterns for *x*wt%Co_3O_4/$Ce_{0.67}Zr_{0.18}Sn_{0.15}O_{2.00}$ catalysts: (a) x = 10.4, (b) 12.7, (c) 16.9, and (d) 19.9 (○: $Ce_{0.67}Zr_{0.18}Sn_{0.15}O_{2.00}$; ■: Co_3O_4).

The composition and BET specific surface area of the *x*Co/CZS catalysts are summarized in Table 2.1. The compositions of the catalysts were confirmed by the XRF analysis to be in good agreement with their stoichiometric values. BET specific surface areas of the *x*Co/CZS catalysts decreased with increasing Co_3O_4 content. These results suggest that some of the Co_3O_4 particles were supported in the pores of $Ce_{0.67}Zr_{0.18}Sn_{0.15}O_{2.00}$.

Table 2.1. Composition and BET surface area of catalysts

Catalyst	Catalyst composition	BET surface area ($m^2\ g^{-1}$)
CZS	$Ce_{0.67}Zr_{0.18}Sn_{0.15}O_{2.00}$	81
10.4Co/CZS	10.4wt%Co_3O_4/$Ce_{0.66}Zr_{0.19}Sn_{0.15}O_{2.00}$	66
12.7Co/CZS	12.7wt%Co_3O_4/$Ce_{0.65}Zr_{0.19}Sn_{0.16}O_{2.00}$	62
16.9Co/CZS	16.9wt%Co_3O_4/$Ce_{0.67}Zr_{0.18}Sn_{0.15}O_{2.00}$	61
19.9Co/CZS	19.9wt%Co_3O_4/$Ce_{0.65}Zr_{0.18}Sn_{0.17}O_{2.00}$	57
16.8Co/CZ	16.8wt%Co_3O_4/$Ce_{0.78}Zr_{0.22}O_{2.00}$	65
16.8Co/CZB	16.8wt%Co_3O_4/$Ce_{0.64}Zr_{0.15}Bi_{0.21}O_{1.895}$	56

Figure 2.3 depicts the temperature dependencies of toluene oxidation over the *x*Co/CZS ($10 \leq x \leq 20$) catalysts. Toluene was completely oxidized into carbon dioxide and steam, and no CO or toluene-derived by-products were detected by gas chromatography-mass spectrometry. The toluene oxidation activity depended on the catalyst composition, and the highest activity was obtained for the 16.9Co/CZS catalyst. Toluene oxidation activity of this catalyst was initially observed at 120 °C, and complete oxidation of toluene was confirmed at 260 °C. The activity decreased when 19.9Co/CZS was applied, probably due to Co_3O_4 agglomeration and particle growth.

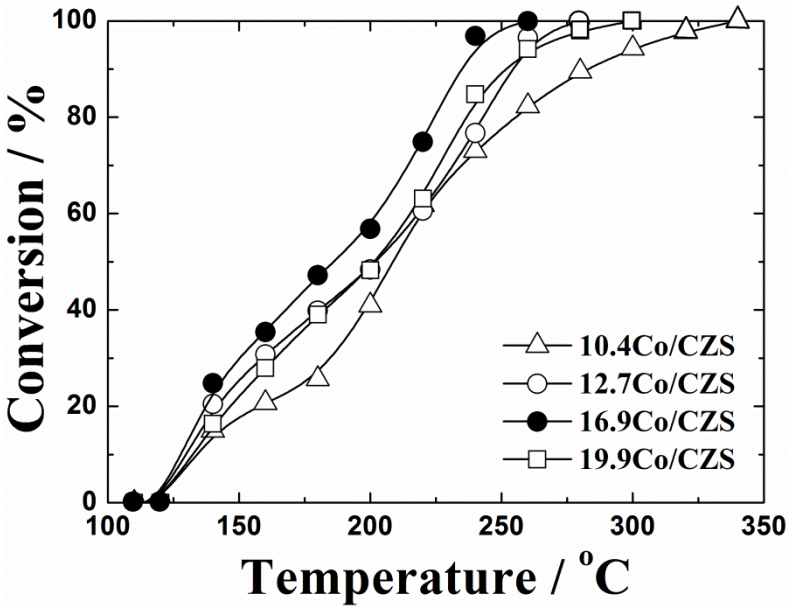

Figure 2.3. Temperature dependencies of toluene conversion on 10.4Co/CZS (△), 12.7Co/CZS (○), 16.9Co/CZS (●), and 19.9Co/CZS (□) catalysts.

Figure 2.4 demonstrates TEM images of the (a) 16.8wt%Co_3O_4/$Ce_{0.78}Zr_{0.22}O_{2.00}$ (16.8Co/CZ), (b) 16.8wt%Co_3O_4/$Ce_{0.64}Zr_{0.15}Bi_{0.21}O_{1.895}$ (16.8Co/CZB), (c) 16.9wt%Co_3O_4/$Ce_{0.67}Zr_{0.18}Sn_{0.15}O_{2.00}$ (16.9Co/CZS), and (d) $Ce_{0.67}Zr_{0.18}Sn_{0.15}O_{2.00}$ (CZSn) samples. As shown in these photographs, there is no clear difference in the size and dispersion state of the particles for each support. In addition, the particle size was about the same before and after the Co_3O_4 deposition on the $Ce_{0.67}Zr_{0.18}Sn_{0.15}O_{2.00}$ support, as recognized from the comparisons of Figure 2.4(c) with (d), which suggests that Co_3O_4 was supported in the pore of the $Ce_{0.67}Zr_{0.18}Sn_{0.15}O_{2.00}$ support.

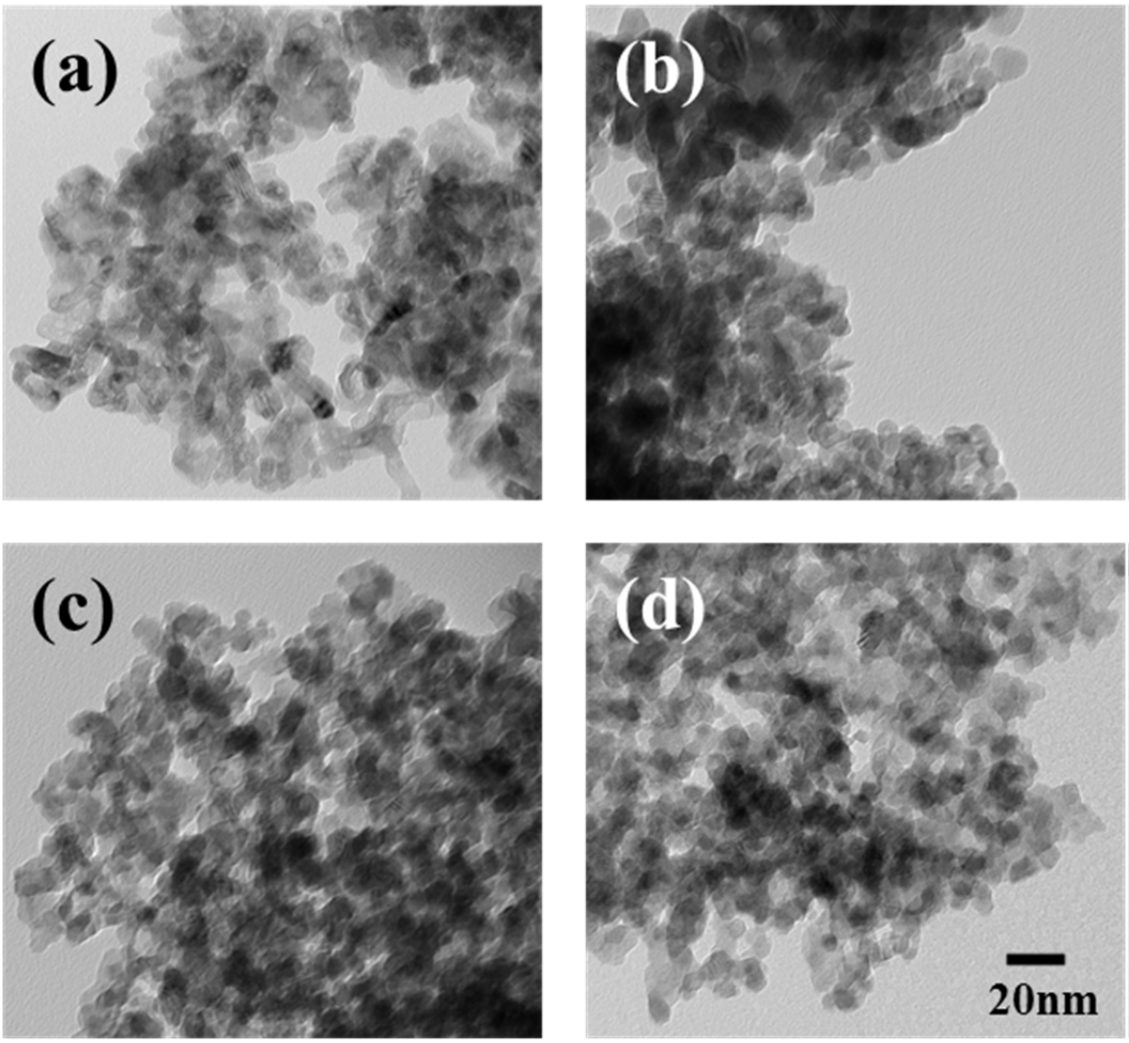

Figure 2.4. TEM photographs of (a) 16.8Co/CZ, (b) 16.8Co/CZB, (c) 16.9Co/CZS, and (d) CZS samples.

The BJH pore size distribution plots of CZS and 16.9Co/CZS are shown in Figure 2.5. As evidenced in this figure, the CZS and 16.9Co/CZS particles have a narrow mesopore size distribution around 6 nm and the size was maintained even if Co_3O_4 was deposited on $Ce_{0.67}Zr_{0.18}Sn_{0.15}O_{2.00}$. However, the pore volume was significantly decreased by the Co_3O_4 deposition, which supports the above discussion.

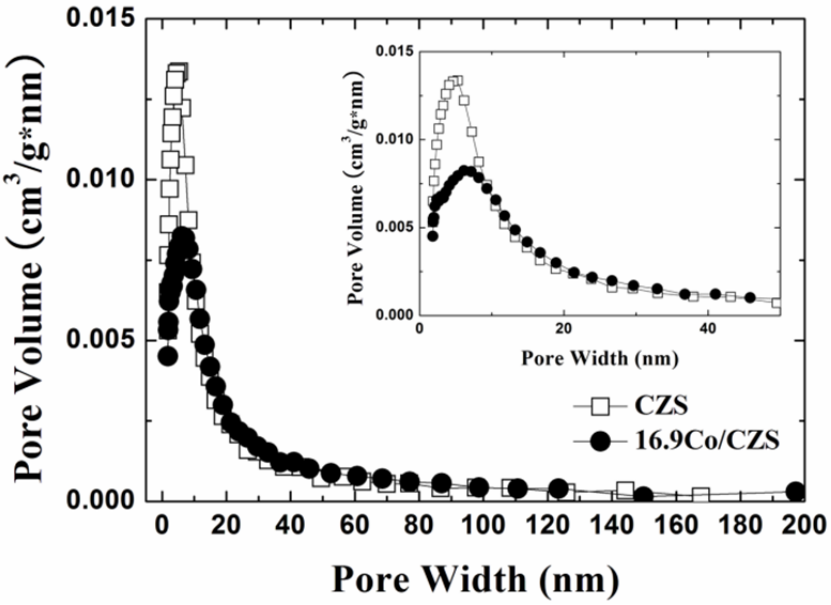

Figure 2.5. BJH pore distribution plots of CZS and 16.9Co/CZS samples.

Figure 2.6(a) shows the temperature dependencies of toluene oxidation over the 16.8wt%Co_3O_4/$Ce_{0.78}Zr_{0.22}O_{2.00}$ (16.8Co/CZ), 16.8wt%Co_3O_4/$Ce_{0.64}Zr_{0.15}Bi_{0.21}O_{1.895}$ (16.8Co/ CZB), and 16.9wt%Co_3O_4/$Ce_{0.67}Zr_{0.18}Sn_{0.15}O_{2.00}$ (16.9Co/CZS) catalysts. As a reference, the profile for the $Ce_{0.67}Zr_{0.18}Sn_{0.15}O_{2.00}$ support was also plotted. Toluene catalytic activity was remarkably promoted not only by the Co_3O_4 introduction, but also by Bi_2O_3 or SnO_2 doping into the CeO_2-ZrO_2 lattice. Among these catalysts, the highest activity was obtained for the 16.9Co/CZS catalyst, over which the complete oxidation of toluene was realized at 260 °C, as mentioned above.

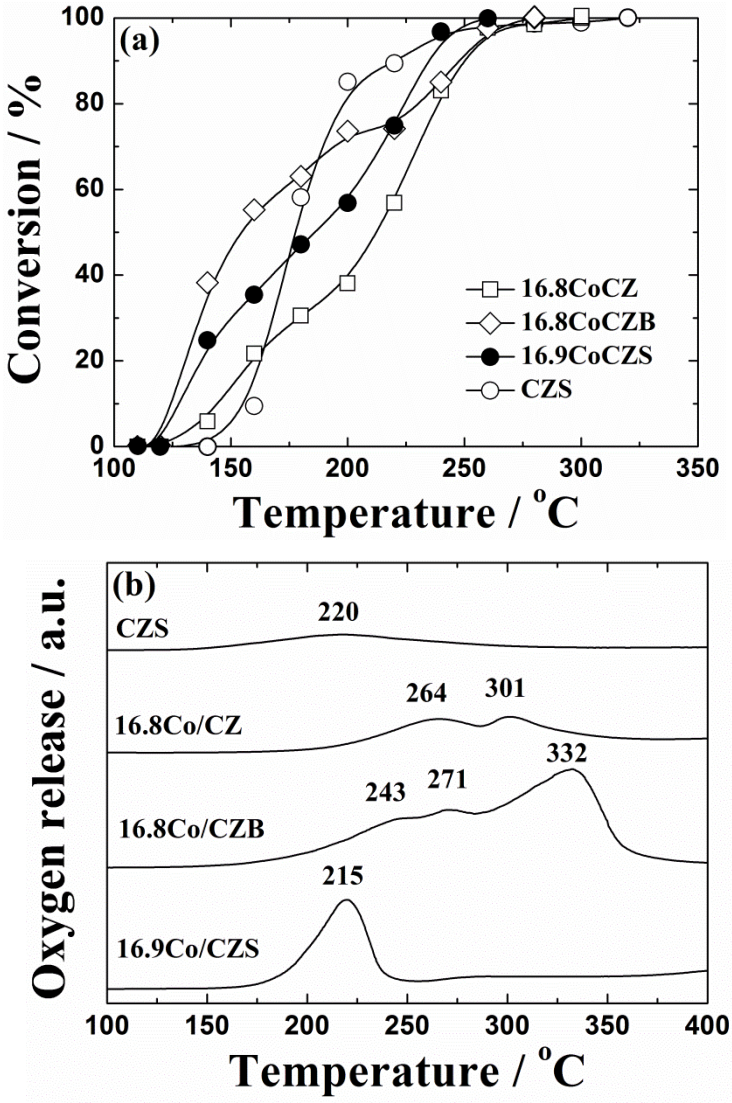

Figure 2.6. Temperature dependencies of (a) toluene conversion and (b) TPR profiles on 16.8Co/CZ (□), 16.8Co/CZB (◇), CZS (○), and 16.9Co/CZS (●) catalysts.

The composition dependence of the oxidation activity of the catalyst can be ascribed to the different reducibility of the supports. To evaluate this hypothesis, TPR profiles were measured for comparison of the reduction behavior of 16.8Co/CZ, 16.8Co/CZB, and 16.9Co/CZS as shown in Figure 2.6(b). As a reference, the TPR profile for the $Ce_{0.67}Zr_{0.18}Sn_{0.15}O_{2.00}$ support was also plotted. The TPR profile of 16.8Co/CZ exhibited two reduction peaks at 264 and 301 °C. For 16.8Co/CZB, reduction initiated at a lower temperature than that for 16.8Co/CZ and reduction peaks were observed at 243, 271, and 332 °C. This promotion of reduction in the low temperature region can be attributed to the high reducibility of Bi_2O_3 and the formation of oxide anion vacancies by partial replacement of the Ce^{4+} and Zr^{4+} sites with Bi^{3+} ions to form solid solutions, leading to the

enhancement of the oxide anion conductivity [29, 36].

In contrast, for 16.9Co/CZS, oxygen release began at a lower temperature than that for 16.8Co/CZB, and a specific reduction peak was observed at 215 °C. Accordingly, the introduction of SnO_2 into the CeO_2-ZrO_2 lattice was remarkably more effective than that of Bi_2O_3 at enhancing the reducibility of the catalyst at lower temperatures, corresponding to high oxidation activity of 16.9Co/CZS. For 16.8Co/CZ and 16.8Co/CZB, Co^{3+}, Ce^{4+}, and Bi^{3+} were reduced separately at different temperatures, while in the case of 16.9Co/CZS, reduction of Co^{3+} to Co^{2+}, Ce^{4+} to Ce^{3+}, and Sn^{4+} to Sn^{2+} occurred at almost the same temperature. As a result, several reduction peaks were observed in 16.8Co/CZ and 16.8Co/CZB, but a single one was observed for 16.9Co/CZS. Since tin ions exist in tetravalent state in $Ce_{0.67}Zr_{0.18}Sn_{0.15}O_{2.00}$ [31], the readily reducible property of the $Ce_{0.67}Zr_{0.18}Sn_{0.15}O_{2.00}$ support can be attributed to the synergistic reduction of Ce^{4+}/Ce^{3+} and Sn^{4+}/Sn^{2+} [53-55].

The oxygen storage capacity (OSC) relevant to the overall reducibility of the catalyst was evaluated by injecting oxygen into the sample reduced by the TPR experiments. The OSC value of 16.9Co/CZS was 1,651 μmol O_2 g^{-1}, which lies midway between those of 16.8Co/CZ (1,350 μmol O_2 g^{-1}) and 16.8Co/CZB (2,079 μmol O_2 g^{-1}). Taking the catalysis and TPR results into account, the high oxidation activity of toluene observed in 16.9Co/CZS can be attributed not to the total oxygen storage capacity but also to the readily reducible property of the $Ce_{0.67}Zr_{0.18}Sn_{0.15}O_{2.00}$ support. The readily reducible Co_3O_4 and $Ce_{0.67}Zr_{0.18}Sn_{0.15}O_{2.00}$ contribute to the provision of active oxygen species from the catalyst bulk, and the oxygen reacts with toluene at the interface of the two Co_3O_4 and $Ce_{0.62}Zr_{0.20}Sn_{0.18}O_{2.00}$ phases. As a result, complete toluene oxidation was realized using the present 16.9Co/CZS catalyst at a temperature of 260 °C, which is lower than those for 16.8Co/CZ (300 °C) and 16.8Co/CZB (280 °C).

For practical applications of the toluene oxidation catalysts, it is important to investigate the impact of water vapor (steam) on the catalytic activities. Steam is a product of toluene oxidation and usually acts as a catalyst poison, because water molecules are adsorbed on the surface of the catalyst. Therefore, the catalytic performance of toluene oxidation in the presence of moisture must be evaluated. The temperature dependencies of toluene oxidation on the 16.9Co/CZS catalyst under dry and moist conditions are shown in Figure 2.7. Also in the moist condition, the reaction products confirmed by gas chromatography-mass spectrometry were only carbon dioxide and steam. As evidenced by these results, the toluene oxidation activity of the 16.9Co/CZS catalyst was unaffected in the presence of saturated water vapor at 0 °C (0.60 vol%) and complete oxidation of toluene was

observed at 260 °C. It is extremely important for the catalysts to maintain their oxidation activity in the presence of moisture for them to be put on the practical use.

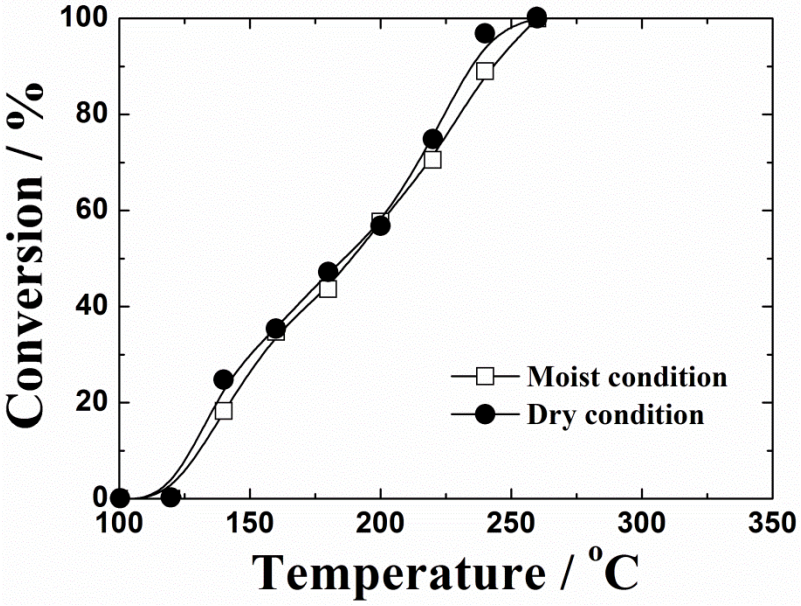

Figure 2.7. Temperature dependencies of toluene combustion to carbon dioxide and steam on 16.9Co/CZS catalyst. Open (○) and closed (●) symbols correspond to data obtained in moist (saturated water vapor at 0 °C; 0.6 vol%) and dry atmospheres, respectively.

2.4. Conclusions

Novel Co_3O_4/CeO_2-ZrO_2-SnO_2 catalysts were successfully prepared by the evaporative drying method and the composition was optimized to give the highest toluene oxidation activity. Catalytic tests for toluene oxidation and characterization of oxygen release/storage properties on these materials showed that the readily reducible property of the CeO_2-ZrO_2-SnO_2 support was significantly effective in facilitating toluene oxidation. In fact, complete oxidation of toluene was realized using the 16.9wt%$Co_3O_4/Ce_{0.67}Zr_{0.18}Sn_{0.15}O_{2.0}$ catalyst at a temperature of 260 °C, which was lower than those for 16.8wt%$Co_3O_4/Ce_{0.78}Zr_{0.22}O_{2.00}$ (300 °C) and 16.8wt%$Co_3O_4/Ce_{0.64}Zr_{0.15}$-$Bi_{0.21}O_{1.895}$ (280 °C). Furthermore, the toluene oxidation activity was maintained even in the presence of moisture. Since Co_3O_4 on the CeO_2-ZrO_2-SnO_2 supports promoted toluene oxidation without using the expensive and rare platinum metal, the 16.9wt%$Co_3O_4/Ce_{0.67}Zr_{0.18}Sn_{0.15}O_{2.00}$ catalyst has potential as a novel environmental catalyst for toluene cleaning at moderate temperatures.

Chapter 3

Catalysts Complete Toluene Oxidation on Pt/CeO_2-ZrO_2-ZnO Catalysts

3.1. Introduction

As mentioned in the Generally Introduction, the catalysis is affected by the influence of dispersed state of active compound and promoters, crystal structure, amount of active species, and surface area of the catalyst [15, 17]. In particular, temperature is also an important parameter that affects the VOCs removal by oxidation catalysis [18]. Moreover, the momentary heat of combustion is to bring over temperature (1000 ^oC) to bear on heat-resisting property of catalyst. Furthermore, thermal stability of the conventional metal-supported catalysts was not satisfactory and new alternative catalysts with high-temperature resistant property have been required.

In previous Chapter 2, my research group found that employing the CeO_2-ZrO_2-Bi_2O_3 and CeO_2-ZrO_2-SnO_2 solid solutions, which have high oxygen release and storage properties, as promoters was effective to establish complete oxidation of VOCs at moderate temperatures [28-30]. In particular, introduction of a small amount of SnO_2, which has been well-known as a typical n-type semiconductor with electronic conduction [32], into the CeO_2-ZrO_2 lattice considerably facilitated the VOCs oxidation [31]. However, thermal stability of the toluene oxidation catalysis on the Co_3O_4/CeO_2-ZrO_2-SnO_2 and Pt/CeO_2-ZrO_2-SnO_2 catalysts was not enough due to readily-reducibility of CoO and SnO_2 respectively.

Accordingly, I focused on the support to using the zinc oxide (ZnO), also known as a stable n-type semiconductor [33] and a 0.4wt%Pt/$Ce_{0.76}Zr_{0.19}Zn_{0.05}O_{1.95}$ catalyst was prepared. Since ZnO has excellent thermal stability, it is expected that thermal stability of the catalyst support will be increased by introducing by ZnO into the CeO_2-ZrO_2 lattice without significant decrease in the catalytic activity.

In Chapter 3, novel Pt/CeO_2-ZrO_2-ZnO catalysts are described, that the catalyst support was introduced the thermal stability of ZnO into the CeO_2-ZrO_2 lattice without significant decrease in the catalytic activity. Therefore, the catalytic toluene oxidation activity of the catalyst was investigated and the calcination temperature dependence on the toluene oxidation activity was also discussed.

3.2. Experimental Procedure

A $Ce_{0.76}Zr_{0.19}Zn_{0.05}O_{1.95}$ solid solution was synthesized by a co-precipitation method. Aqueous solutions of 1.0 mol dm^{-3} $Ce(NO_3)_3$ (9.5 cm^3), 0.1 mol dm^{-3} $ZrO(NO_3)_2$ (23.75 cm^3), and 0.1 mol dm^{-3} $Zn(NO_3)_2$ (6.25 cm^3) were mixed with 3.0 mol dm^{-3} HNO_3 (100 cm^3) in a stoichiometric ratio, and polyvinylpyrrolidone K25 (PVP; Wako Pure Chemical Industries, Ltd., Osaka, Japan, mean molecular weight is 35,000 and mean degree of polymerization is 315) was also dissolved into the mixture. The molar ratio of total metal cations to PVP was 31.5. Then, the solution was stirred at 80 °C for 6 h. After the solvent was evaporated at 180 °C, the resulting powder was heated at 350 °C for 4 h to remove PVP and then calcined at 500 °C for 1 h. A supported 0.4wt%Pt/$Ce_{0.76}Zr_{0.19}Zn_{0.05}O_{1.95}$ catalyst was prepared by impregnating the $Ce_{0.76}Zr_{0.19}Zn_{0.05}O_{1.95}$ support with a platinum colloid stabilized with PVP (Tanaka Kikinzoku Kogyo Co., Ltd, Tokyo, Japan). After impregnation, the catalyst was dried at 80 °C for 12 h and then finally calcined at 500, 700, 900 and 1000 °C for 4 h. For references, 0.4wt%Pt/ $Ce_{0.79}Zr_{0.21}O_{2.00}$ and 0.4wt%Pt/$Ce_{0.73}Zr_{0.21}Sn_{0.06}O_{2.00}$ catalysts were also prepared using the same procedure.

The sample compositions were analyzed using an X-ray fluorescence spectrometer (XRF; Rigaku, ZSX-100e). The crystal structures of the catalysts were identified by X-ray powder diffraction (XRD; Rigaku, SmartLab, Tokyo, Japan) using Cu-Kα radiation (40 kV, 30mA). The Brunauer-Emmett-Teller (BET) specific surface area was measured by nitrogen adsorption at −196 °C (MicromeriticsTristar 3000, Norcross GA, USA). Temperature programmed reduction (TPR) measurements were carried out under a flow of 5 vol% H_2-Ar (50 cm^3 min^{-1}) at a heating rate of 5 °C min^{-1} and the platinum dispersion analysis was carried out by a pulse method at -50 °C using 10% CO-He (0.03 cm^3) with a BELCAT-B apparatus (BEL, Osaka, Japan).

The oxidation activity for toluene was tested by the similar procedure described in Chapter 1. The feed gas was composed of 0.09 vol% toluene in an air balance and the rate was 20 cm^3 min^{-1} over 0.1 g of the catalyst, where the space velocity is 12,000 dm^{-3} kg^{-1} h^{-1}.

3.3. Results and Discussion

Figure 3.1 shows the X-ray powder diffraction (XRD) patterns of the 0.4wt%Pt/$Ce_{0.76}Zr_{0.19}Zn_{0.05}O_{1.95}$ catalysts calcined at 500, 700, 900 and 1000 °C. The XRD patterns of the catalysts contain diffraction peaks of only the cubic fluorite-type oxide, and no peaks corresponding to platinum were observed probably due to its low content. The diffraction peaks assigned to the cubic fluorite-type structure were steady and no peak shift was observed regardless of the calcination temperature, indicating that platinum was supported on the surface of the $Ce_{0.76}Zr_{0.19}Zn_{0.05}O_{1.95}$ support without forming solid solutions. The composition of the catalyst was confirmed by the X-ray fluorescence spectrometer (XRF) analysis to be in good agreement with their stoichiometric value. The BET specific surface area of the 0.4wt%Pt/$Ce_{0.76}Zr_{0.19}Zn_{0.05}O_{1.95}$ catalysts decreased from 33 $m^2\ g^{-1}$ to 0.9 $m^2\ g^{-1}$ with increasing the calcination temperature, as summarized in Table 3.1. A drop in platinum dispersion was also observed with raising calcination temperature.

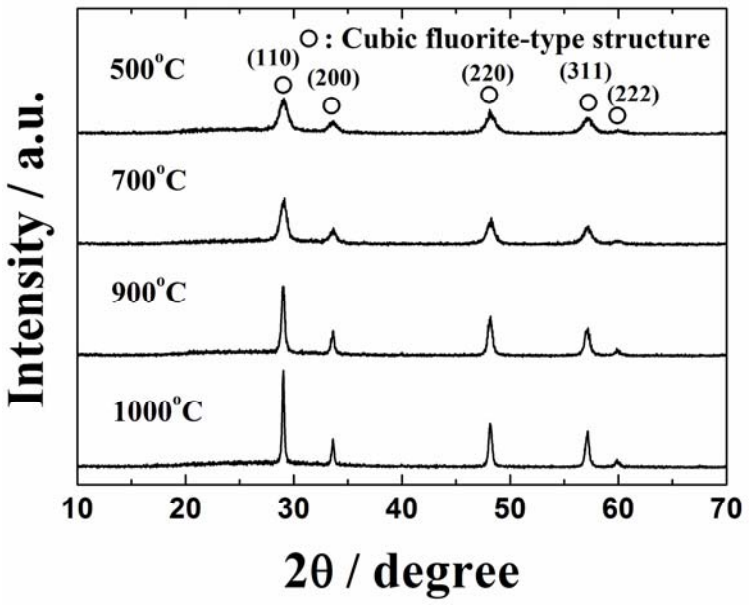

Figure 3.1. X-ray powder diffraction (XRD) patterns of the 0.4wt%Pt/$Ce_{0.76}Zr_{0.19}Zn_{0.05}O_{1.95}$ catalysts calcined at 500, 700, 900 and 1000 °C.

Table 3.1. Brunauer-Emmett-Teller (BET) surface area of the 0.4wt%Pt/$Ce_{0.76}Zr_{0.19}Zn_{0.05}O_{1.95}$ catalysts.

Catalyst composition	Calcination temperature (°C)	BET surface area (m^2 g^{-1})	Pt dispersion (%)
0.4wt%Pt/$Ce_{0.76}Zr_{0.19}Zn_{0.05}O_{1.95}$	500	33	63
0.4wt%Pt/$Ce_{0.76}Zr_{0.19}Zn_{0.05}O_{1.95}$	700	21	22
0.4wt%Pt/$Ce_{0.76}Zr_{0.19}Zn_{0.05}O_{1.95}$	900	4.5	2.3
0.4wt%Pt/$Ce_{0.76}Zr_{0.19}Zn_{0.05}O_{1.95}$	1000	0.9	2.0

On the other hand, in the case of 0.4wt%Pt/$Ce_{0.73}Zr_{0.21}Sn_{0.06}O_{2.00}$ catalysts, in which SnO_2 was introduced into CeO_2-ZrO_2 instead of ZnO, small SnO_2 peaks were observed as the secondary impurity phase for the samples calcined at 900 and 1000 °C, as depicted in Figure 3.2. From these results, it has been evidenced that the thermal stability of the zinc-doped catalyst (0.4wt%Pt/$Ce_{0.76}Zr_{0.19}Zn_{0.05}O_{1.95}$) is higher than that of the tin-doped catalyst (0.4wt%Pt/$Ce_{0.73}Zr_{0.21}Sn_{0.06}O_{2.00}$).

Figure 3.3 shows the temperature dependencies of toluene oxidation over the 0.4wt%Pt/$Ce_{0.76}Zr_{0.19}Zn_{0.05}O_{1.95}$ catalysts calcined at 500, 700, 900 and 1000 °C. It was confirmed that only carbon dioxide and steam were produced by the complete oxidation of toluene, and neither CO nor toluene-derived compounds were detected as by-products with a gas chromatography-mass spectrometer. Toluene was completely oxidized at 320 °C on the 0.4wt%Pt/$Ce_{0.76}Zr_{0.19}Zn_{0.05}O_{1.95}$ catalyst calcined at 500 °C. The toluene oxidation activity decreased with increasing the calcination temperature, because of the decrease in the BET specific surface area. However, significant deactivation was not recognized in the present 0.4wt%Pt/$Ce_{0.76}Zr_{0.19}Zn_{0.05}O_{1.95}$ catalyst, and toluene was completely oxidized at 360 °C even after calcination at 1000 °C.

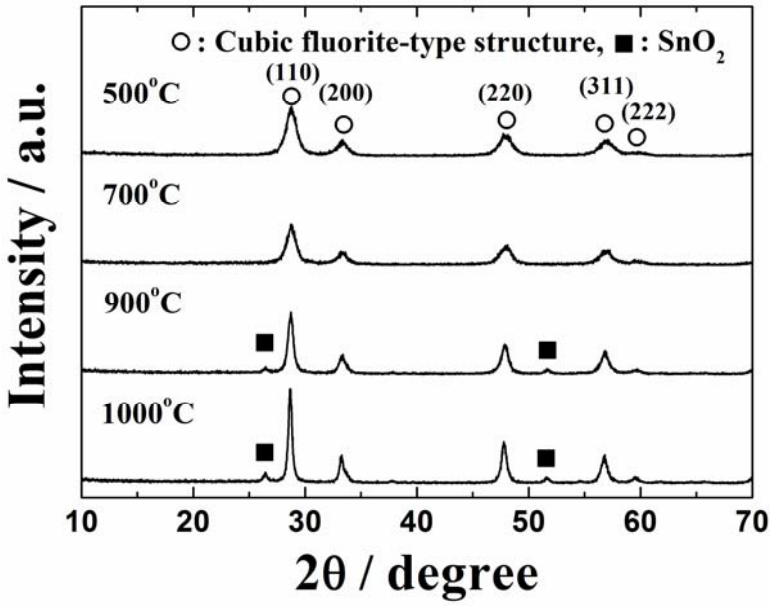

Figure 3.2. XRD patterns of the 0.4wt%Pt/$Ce_{0.73}Zr_{0.21}Sn_{0.06}O_{2.00}$ catalysts calcined at 500, 700, 900 and 1000 °C.

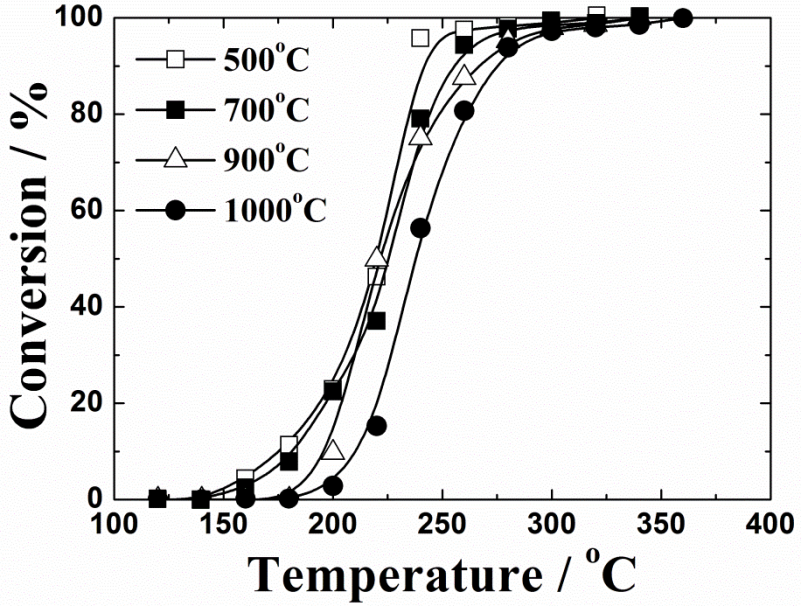

Figure 3.3. Temperature dependencies of toluene oxidation on the 0.4wt%Pt/$Ce_{0.76}Zr_{0.19}Zn_{0.05}O_{1.95}$ catalysts calcined at 500, 700, 900 and 1000 °C.

The catalytic activity and thermal stability of 0.4wt%Pt/$Ce_{0.76}Zr_{0.19}Zn_{0.05}O_{1.95}$ was compared with those of 0.4wt%Pt/$Ce_{0.73}Zr_{0.21}Sn_{0.06}O_{2.00}$ and a conventional dopant-free 0.4wt%Pt/$Ce_{0.79}Zr_{0.21}O_{2.00}$ catalyst. The complete oxidation temperatures of toluene over these catalysts are summarized in Table 3.2. Among the catalysts calcined at 500 °C,

0.4wt%Pt/$Ce_{0.73}Zr_{0.21}Sn_{0.06}O_{2.00}$ was the most active catalyst. However, this catalyst was significantly deactivated after the calcination at 1000 °C and the toluene oxidation temperature was increased up to 460 °C, which was higher by 100 °C than that of 0.4wt%Pt/$Ce_{0.76}Zr_{0.19}Zn_{0.05}O_{1.95}$. The 0.4wt%Pt/$Ce_{0.79}Zr_{0.21}O_{2.00}$ catalyst had the lowest activities at both calcination temperatures. As a result, it is evident that the 0.4wt%Pt/$Ce_{0.76}Zr_{0.19}Zn_{0.05}O_{1.95}$ catalyst has the highest thermal stability for toluene oxidation among these catalysts.

Table 3.2. Complete oxidation temperature of toluene on the catalysts calcined at 500 and 1000 °C.

Catalyst composition	Calcination temperature (°C)	Complete oxidation temperature of toluene (°C)
0.4wt%Pt/$Ce_{0.79}Zr_{0.21}O_{2.00}$	500	340
0.4wt%Pt/$Ce_{0.79}Zr_{0.21}O_{2.00}$	1000	480
0.4wt%Pt/$Ce_{0.73}Zr_{0.21}Sn_{0.06}O_{2.00}$	500	260
0.4wt%Pt/$Ce_{0.73}Zr_{0.21}Sn_{0.06}O_{2.00}$	1000	460
0.4wt%Pt/$Ce_{0.76}Zr_{0.19}Zn_{0.05}O_{1.95}$	500	320
0.4wt%Pt/$Ce_{0.76}Zr_{0.19}Zn_{0.05}O_{1.95}$	1000	360

The results in Table 2 suggest that the thermal stability of the catalytic activity was improved by the presence of zinc. To identify the reason for the positive effect of the zinc doping, temperature programmed reduction (TPR) spectra were measured for $Ce_{0.76}Zr_{0.19}Zn_{0.05}O_{1.95}$ and $Ce_{0.73}Zr_{0.21}Sn_{0.06}O_{2.00}$ after the calcination at 1000 °C, and their oxygen release behaviors were compared as shown in Figure 3.4. For the $Ce_{0.76}Zr_{0.19}Zn_{0.05}O_{1.95}$ support, the strong reduction peaks were observed at 542 °C and 841 °C, while for the $Ce_{0.73}Zr_{0.21}Sn_{0.06}O_{2.00}$ one, a small and a main reduction peaks were observed at 352 °C and 616 °C, respectively. It is noteworthy that the main reduction peak for the former at 542 °C was lower by approximately 80 °C than that of the latter (616 °C), and introduction of ZnO into the CeO_2-ZrO_2 lattice was obviously more effective than that of SnO_2 to inhibit the thermal degradation of the catalyst support. Therefore, the complete toluene oxidation temperature for 0.4wt%Pt/$Ce_{0.76}Zr_{0.19}Zn_{0.05}O_{1.95}$ (360 °C) became lower than that of 0.4wt%Pt/$Ce_{0.73}Zr_{0.21}Sn_{0.06}O_{2.00}$ (460 °C) after heating at 1000 °C. From a comprehensive consideration of the XRD, catalysis, and TPR results, it was found that thermal stability of the support is particularly important to preserve the activity even after high-temperature firing.

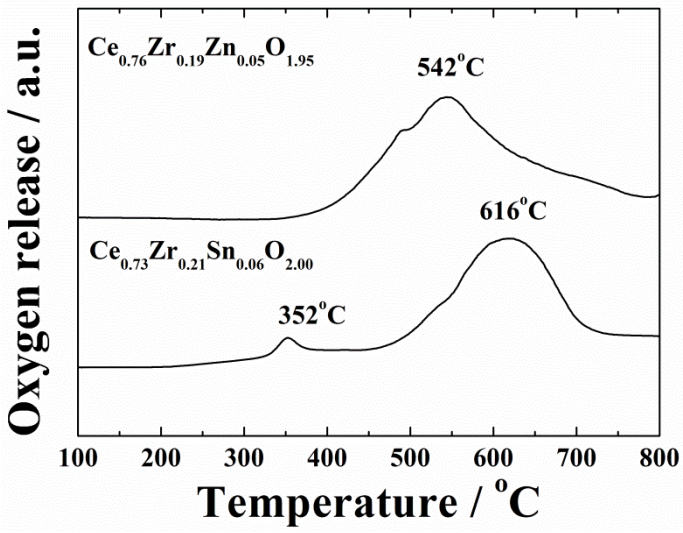

Figure 3.4. Temperature programmed reduction (TPR) profiles of the $Ce_{0.76}Zr_{0.19}Zn_{0.05}O_{1.95}$ and $Ce_{0.73}Zr_{0.21}Sn_{0.06}O_{2.00}$ supports calcined at 1000 °C.

Figure 3.5 depicts the temperature dependencies of toluene oxidation over the $Ce_{0.76}Zr_{0.19}Zn_{0.05}O_{1.95}$ and $Ce_{0.73}Zr_{0.21}Sn_{0.06}O_{2.00}$ supports calcined at 1000 °C. It was confirmed in these cases that only carbon dioxide and steam were produced by the complete oxidation of toluene, and neither CO nor toluene-derived compounds were detected as by-products. The catalytic activity was remarkably promoted by the ZnO doping into the CeO_2-ZrO_2 lattice. These results correspond to the TPR results discussed above and apparently show the advantage of the ZnO doping to improve the thermal stability of the support.

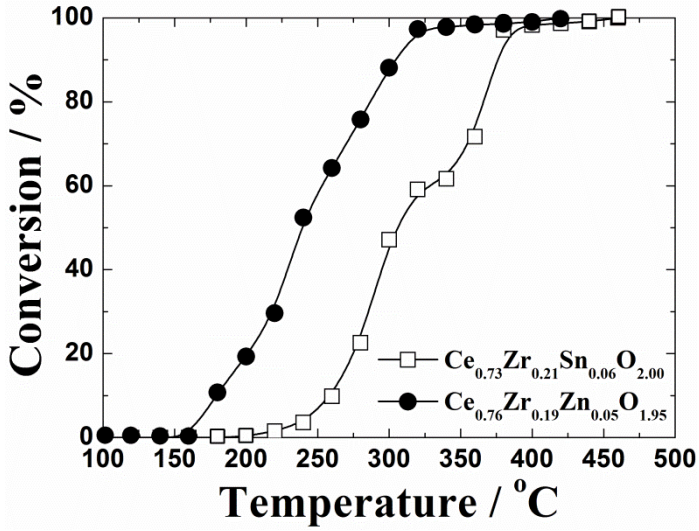

Figure 3.5. Temperature dependencies of toluene oxidation on $Ce_{0.76}Zr_{0.19}Zn_{0.05}O_{1.95}$ and $Ce_{0.73}Zr_{0.21}Sn_{0.06}O_{2.00}$ supports calcined at 1000 °C.

Figure 3.6 shows TPR spectra of 0.4wt%Pt/$Ce_{0.76}Zr_{0.19}Zn_{0.05}O_{1.95}$ and 0.4wt%Pt/ $Ce_{0.73}Zr_{0.21}Sn_{0.06}O_{2.00}$ after the calcination at 1000 °C. The reduction onset temperature of 0.4wt%Pt/$Ce_{0.76}Zr_{0.19}Zn_{0.05}O_{1.95}$ (367 °C) was higher than that of 0.4wt%Pt/$Ce_{0.73}Zr_{0.21}Sn_{0.06}O_{2.00}$ (214 °C). However, reduction of the former was almost completed at 500 °C, while a main peak was observed at 572 °C for the latter: relatively larger amount of lattice oxygen was released for 0.4wt%Pt/$Ce_{0.76}Zr_{0.19}Zn_{0.05}O_{1.95}$ at 500 °C or below. The difference of the reduction behavior will be responsible for higher activity of 0.4wt%Pt/$Ce_{0.76}Zr_{0.19}Zn_{0.05}O_{1.95}$ after heating at 1000 °C.

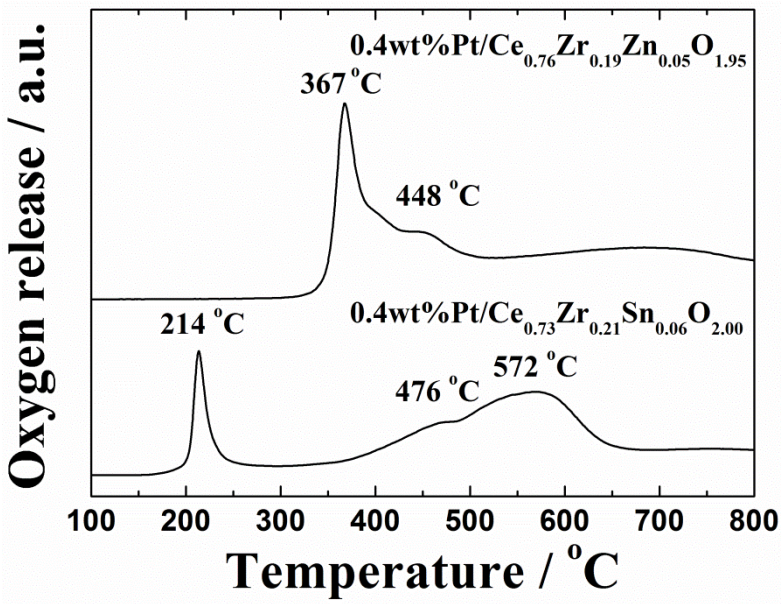

Figure 3.6. TPR profiles of 0.4wt%Pt/$Ce_{0.76}Zr_{0.19}Zn_{0.05}O_{1.95}$ and 0.4wt%Pt/$Ce_{0.73}Zr_{0.21}Sn_{0.06}O_{2.00}$ calcined at 1000 °C.

The catalytic test up to 1000 °C was repeated three times to evaluate thermal stability of the 0.4wt%Pt/$Ce_{0.76}Zr_{0.19}Zn_{0.05}O_{1.95}$ catalyst. As demonstrated in Figure 3.7, it was confirmed that the catalyst was stable and was not deactivated throughout the repeated use of the catalyst: 100% conversion of toluene to carbon dioxide and steam was sustained and carbon deposition was not observed. Furthermore, neither CO nor H_2 were detected as by-products by gas chromatography mass spectrometry and there were no side reactions such as imperfect combustion and partial oxidation. As a result, it became obvious that the 0.4wt%Pt/$Ce_{0.76}Zr_{0.19}Zn_{0.05}O_{1.95}$ catalyst has high thermal stability for toluene oxidation.

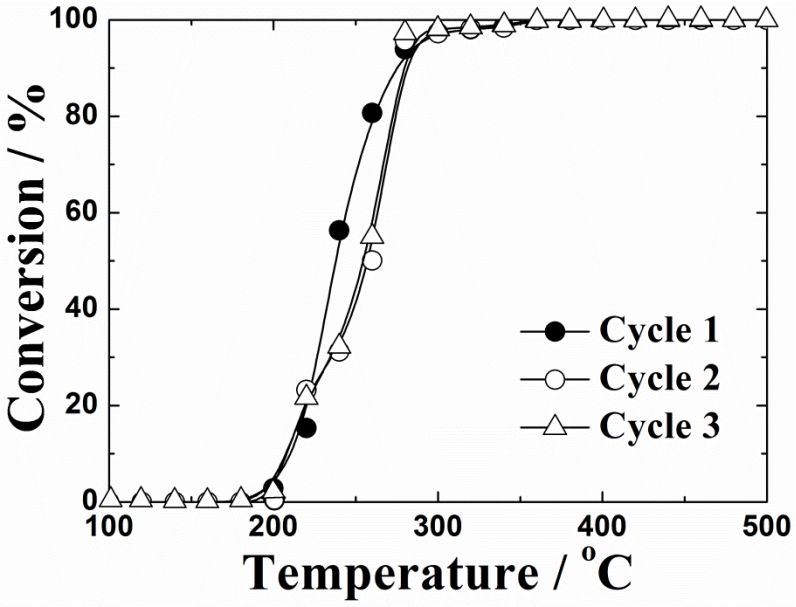

Figure 3.7. Measurement of the thermal stability by the temperature dependencies of toluene oxidation over the 0.4wt%Pt/$Ce_{0.76}Zr_{0.19}Zn_{0.05}O_{1.95}$ catalyst calcined at 1000 °C.

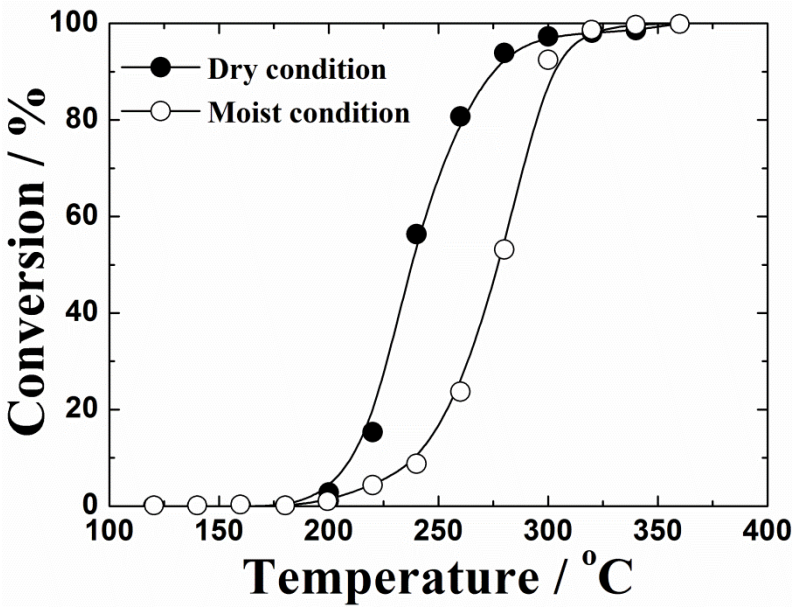

Figure 3.8. Temperature dependencies of toluene combustion to carbon dioxide and steam on the 0.4wt%Pt/$Ce_{0.76}Zr_{0.19}Zn_{0.05}O_{1.95}$ catalyst calcined at 1000 °C. Open (○) and closed (●) symbols correspond to data obtained in moist (saturated water vapor at 0 °C; 0.6 vol%) and dry atmospheres, respectively.

For practical applications of the toluene oxidation catalysts, it is important to investigate the impact of water vapor (steam) on the catalytic activities. Steam is a product of toluene oxidation and usually acts as a catalyst poison, because water molecules are adsorbed on the surface of the catalyst. Therefore, the catalytic performance of toluene oxidation in the presence of moisture must be evaluated. The temperature dependencies of toluene oxidation on the 0.4wt%Pt/$Ce_{0.76}Zr_{0.19}$-$Zn_{0.05}O_{1.95}$ catalyst calcined at 1000 °C under dry and moist conditions are shown in Figure 3.8. Also in the moist condition, the reaction products confirmed by gas chromatography-mass spectrometry were only carbon dioxide and steam. Although the light off behavior of the toluene oxidation activity of the 0.4wt%Pt/$Ce_{0.76}Zr_{0.19}Zn_{0.05}O_{1.95}$ catalyst was slightly decreased in the presence of saturated water vapor at 0 °C (0.60 vol%), complete oxidation temperature of toluene was maintained at 360 °C. It is extremely important for the catalysts to maintain the complete reaction temperature in the presence of moisture to put them on the practical use.

3.4. Conclusions

The novel Pt/CeO_2-ZrO_2-SnO_2 and Pt/CeO_2-ZrO_2-ZnO catalysts were successfully prepared by the evaporative drying method. Catalytic tests for toluene oxidation and characterization of oxygen release/storage properties on these materials showed that the thermal stability of the CeO_2-ZrO_2-ZnO support was significantly effective in facilitating toluene oxidation even after high-temperature calcination at 1000 °C. In fact, complete oxidation of toluene was realized at a temperature of 360 °C using the 0.4wt%Pt/$Ce_{0.76}Zr_{0.19}Zn_{0.05}O_{1.95}$ catalyst calcined at 1000 °C, where the temperature was lower than that for 0.4wt%Pt/$Ce_{0.73}Zr_{0.21}Sn_{0.06}O_{2.00}$ (460 °C) calcined at 1000 °C. Furthermore, the toluene oxidation activity was maintained even in the presence of moisture.

Chapter 4

Complete Oxidation of Toluene on refractory $La_{1-x}Ca_xCoO_{3-x/2}/CeO_2$-$ZrO_2$-ZnO catalysts

4.1. Introduction

As described in Chapters 1 and 3, high toluene oxidation activity was realized by the combination of platinum and active oxygen supplied from the CeO_2-ZrO_2-SnO_2 and CeO_2-ZrO_2-ZnO supports. However, the conventional Pt-supported catalysts usually deactivate after being exposed to high temperatures of the combustion heat over 1000 °C due to aggregation and growth of the platinum particles, in spite of platinum being a precious metal. Therefore, there is a real need for a novel oxidation catalyst with high-temperature endurance [21-23].

In previous studies conducted by the research group, to which I belong it was applied solid solutions as promoters that have high oxygen release and storage abilities to establish complete oxidation of VOCs at moderate temperatures [28-31, 56-58]. In particular, introduction of a small amount of ZnO, which has been well-known as a typical n-type semiconductor with electronic conduction [33, 59], into the CeO_2-ZrO_2 lattice considerably facilitated the toluene oxidation.

Figure 4.1 shows temperature dependencies of toluene oxidation on 0.4wt%Pt/$Ce_{0.76}Zr_{0.19}$-$Zn_{0.05}O_{1.95}$ catalyst calcined at 1000 °C and 1400 °C. In the case of the 0.4wt%Pt/$Ce_{0.76}Zr_{0.19}$-$Zn_{0.05}O_{1.95}$ catalyst, the catalyst was deactivated by the high temperature sintering of the platinum particles. Actually, it was evidenced that toluene was completely oxidized into carbon dioxide and steam at 360 °C on a 0.4wt%Pt/$Ce_{0.76}Zr_{0.19}Zn_{0.05}O_{1.95}$ catalyst after calcination at 1000 °C [58]. However, this catalyst deactivated when it was calcined at 1400 °C.

Accordingly, temperature differential between complete toluene oxidation and catalyst calcination (ΔT) on this catalyst was only 640 °C. Since toluene oxidation catalysts are often subjected under significantly high temperature conditions by the local combustion heat, it is necessary for such catalysts to have high thermal stability even after being subjected to temperature from over 1000 °C up to around 1400 °C. Therefore, further advancement of the thermal stability of the catalyst is required to obtain a considerably higher ΔT value than 1000 °C. For that purpose, platinum is not a suitable candidate due to easy aggregation over 1000 °C. In addition, the use of platinum usually has high production costs, making it prohibitive from a practical application

standpoint. Therefore, it is desirable to develop catalysts free from platinum without a significant decrease in the catalytic activity.

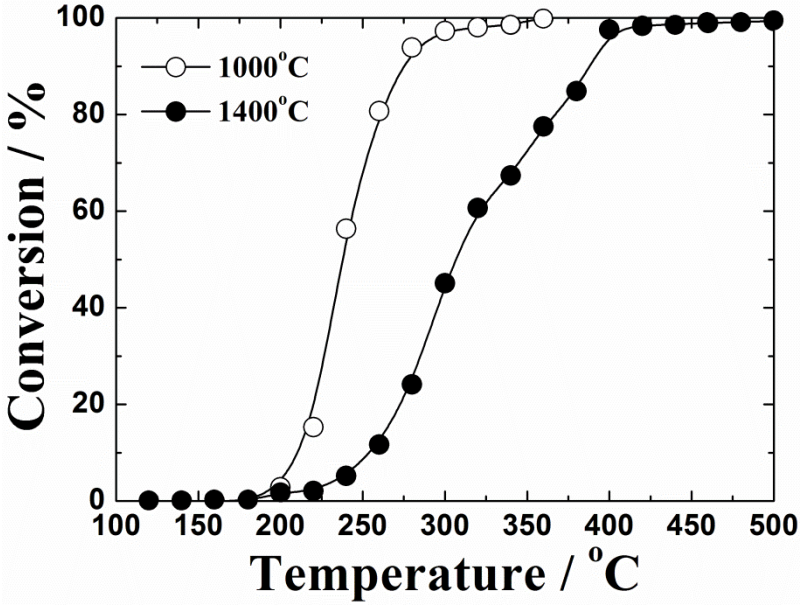

Figure 4.1. Temperature dependencies of toluene oxidation on 0.4wt%Pt/$Ce_{0.76}Zr_{0.19}Zn_{0.05}O_{1.95}$ catalyst calcined at 1000 °C (○) and 1400 °C (●).

To realize such advanced catalysts, I focused on perovskite-type lanthanum cobaltate ($LaCoO_3$). The perovskite-type structure is generally described by the formula ABO_3, where A and B are usually alkaline earth, rare earth, and transition metal cations. Their catalytic properties are closely related to the nature of the B-site cation [60]. The oxygen nonstoichiometry and mobility inside the perovskite lattice are affected by the A-site cation [61]. Typically, the B-site cation is 6 fold and the A-site cation is 12 fold coordinated with O^{2-} ions. Furthermore, the partial substitution of the A or B ion is possible considering these conditions which offer an enormous amount of different compositions. The defects of cations and anions result in frequently observed nonstoichiometry of the system. Due to their variable and broad range of chemical compositions but also because of the well controllable physical and chemical properties and a high thermal stability perovskite-type structures are excellent model compounds in chemical research especially in catalysis.

Therefore, for reasons mentioned above, I used to perovskite-type lanthanum cobaltate ($LaCoO_3$) instead of platinum as the catalyst to facilitate toluene oxidation, because $LaCoO_3$ shows a gradual insulator-metal transition at about 230 °C [62], and, due to this induced metallic property,

it is expected that $LaCoO_3$ can work as an alternative to Pt. In addition, $LaCoO_3$ has been reported to have catalytic activity for toluene oxidation and excellent thermal stability [63]. Furthermore, the excellent performance of perovskite-type structures in oxidation catalysis is closely related to the surface defects being generated by cation and anion deficiencies or by defects generated by partial substitution of the cations [60, 61]. These sites are preferential points for O_2 adsorption and step-wise charge transfer to generate catalytically active oxygen species. Therefore, introduction of oxide ion defects by Ca^{2+} doping in the La^{3+} sites will enhance the oxide anion mobility to facilitate toluene oxidation.

In Chapter 4, novel *y*wt%$La_{1-x}Ca_xCoO_{3-x/2}$/$Ce_{0.76}Zr_{0.19}Zn_{0.05}O_{1.95}$ catalysts ($0 \leq x \leq 0.15$), which the catalytic combustion of toluene on the catalysts was described to realize complete abatement of toluene at as low temperature as possible, leading to the enhancement of ΔT of the catalysts was also discussed.

4.2. Experimental Procedure

$La_{1-x}Ca_xCoO_{3-x/2}$ ($0 \leq x \leq 0.15$) perovskite oxides were synthesized by the conventional solid state reaction method. La_2O_3, CoO and $CaCO_3$ were mixed in a stoichiometric ratio using an agate mortar, and then the powder was mechanically mixed for 3 h using a planetary ball-milling apparatus (Fritsch, Pulverisette 7). The homogenous mixture was first calcined at 800 °C for 4 h and then the calcined powder was pulverized again by ball-mill crushing for 3 h. Finally, the sample was calcined at 1400 °C for 4 h.

The $Ce_{0.76}Zr_{0.19}Zn_{0.05}O_{1.95}$ solid solution was prepared by the similar procedure described in Chapter 3. Finally, the perovskite $La_{1-x}Ca_xCoO_{3-x/2}$ oxides were supported on the $Ce_{0.76}Zr_{0.19}$-$Zn_{0.05}O_{1.95}$ solid solution, where the amount of $La_{1-x}Ca_xCoO_{3-x/2}$ was adjusted to 15~20wt%, and the catalyst was calcined at 1400 °C for 4 h.

The crystal structure of the catalysts was identified by X-ray powder diffraction (XRD; Rigaku, SmartLab) using Cu-Kα radiation (40 kV, 30 mA). The sample composition was analyzed by using X-ray fluorescence spectrometry (XRF; Rigaku, ZSX-100e). The Brunauer-Emmett-Teller (BET) specific surface area was measured by nitrogen adsorption at −196 °C (Micromeritics, Tristar 3000). The microstructure of the catalyst was observed with a scanning electron microscope (SEM; Shimadzu, SSX-550). The sample was sputter-coated with a platinum layer before SEM observation to avoid any possible surface charging effects. X-ray photoelectron spectroscopy (XPS; ULVAC

5500MT) measurement was performed at room temperature using Mg-Kα radiation (1253.6 eV). The effect of charging on the binding energies was corrected with respect to the C 1s peak at 284.6 eV. Temperature programmed reduction (TPR) measurements were carried out under a flow of 5 vol% H_2-Ar (50 cm^3 min^{-1}) at a heating rate of 5 °C min^{-1} (BEL JAPAN, BELCAT-B). Following the TPR experiments, the total oxygen storage capacity (OSC) relevant to the overall reducibility of the catalyst was measured using a pulse-injection method at 427 °C.

The oxidation activity for toluene was tested by the similar procedure described in Chapter 1. The feed gas was composed of 0.09 vol% toluene in an air balance and the rate was 20 cm^3 min^{-1} over 0.1 g of the catalyst, where the space velocity is 15,000 dm^{-3} kg^{-1} h^{-1}.

4.3. Results and Discussion

Figure 4.2 shows XRD patterns of the $La_{1-x}Ca_xCoO_{3-x/2}$ ($0 \leq x \leq 0.15$) samples synthesized at 1400 °C. A single-phase perovskite-type lanthanum cobaltate ($LaCoO_3$) structure was observed for all the catalysts, no diffraction peaks of impurities were evident in the patterns. As seen in the enlargement of the patterns in the 2θ range from 58 to 60°, the XRD peaks shifted to higher angles with increasing Ca^{2+} content, because La^{3+} (ionic radius: 0.136 nm) [52] in the host lattice is partially substituted by smaller Ca^{2+} (ionic radius: 0.134 nm) [52] ions. The lattice volumes of the $La_{1-x}Ca_xCoO_{3-x/2}$ samples calculated from the diffraction angles in the XRD patterns are summarized in Table 4.1. The lattice volume of the perovskite phase decreased monotonically with increasing Ca^{2+} concentration, which indicates the formation of solid solutions.

Table 4.1. Lattice volume of the $La_{1-x}Ca_xCoO_{3-x/2}$ samples synthesized at 1400 °C.

Sample	Lattice volume / nm^3
$LaCoO_3$	0.3881
$La_{0.96}Ca_{0.03}CoO_{2.985}$	0.3754
$La_{0.94}Ca_{0.07}CoO_{2.965}$	0.3649
$La_{0.90}Ca_{0.10}CoO_{2.950}$	0.3507
$La_{0.88}Ca_{0.12}CoO_{2.940}$	0.3320
$La_{0.85}Ca_{0.15}CoO_{2.925}$	0.3078

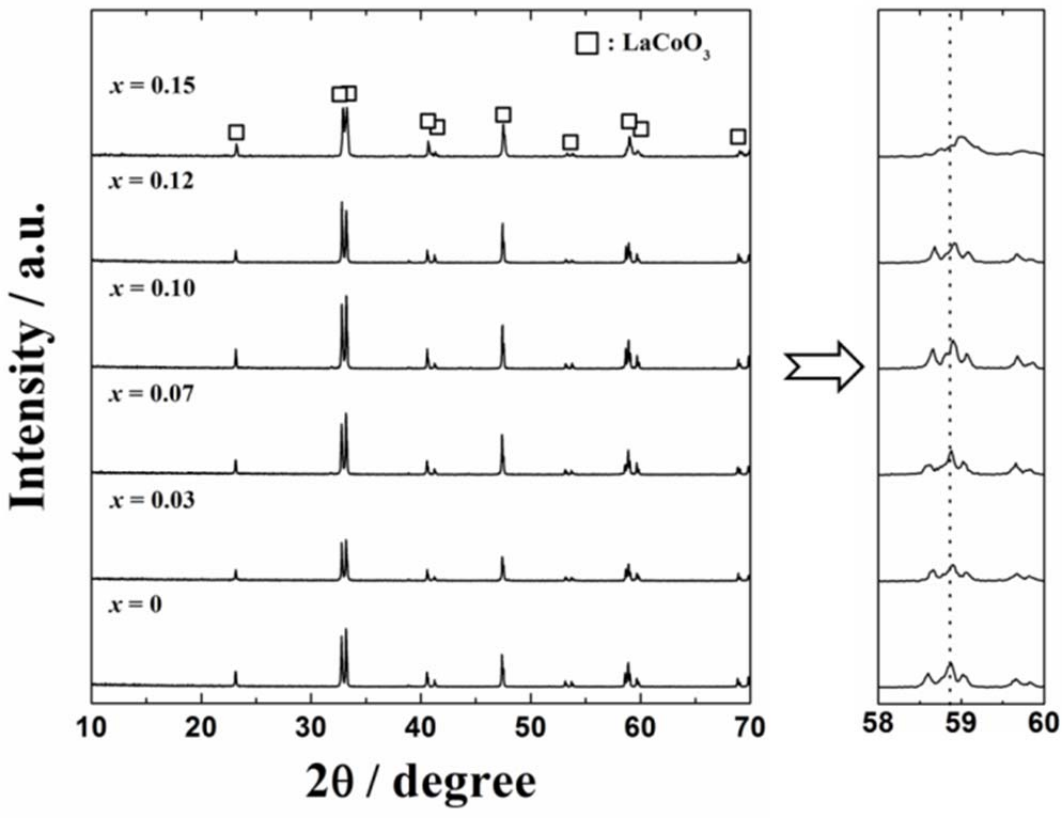

Figure 4.2. XRD patterns of the $La_{1-x}Ca_xCoO_{3-x/2}$ samples synthesized at 1400 °C.

To optimize the amount of the perovskite-type $La_{1-x}Ca_xCoO_{3-x/2}$ oxide, composition dependencies of complete oxidation temperature of toluene was measured preliminarily for the *y*wt%$La_{0.9}Ca_{0.1}CoO_{2.95}$/$Ce_{0.76}Zr_{0.19}Zn_{0.05}O_{1.95}$ (*y* = 15, 17, and 20) catalysts prepared at 1400 °C, as summarized in Table 4.2. Toluene was completely oxidized into carbon dioxide and steam, and no CO or toluene-derived by-products were detected. The complete oxidation temperature depended on the catalyst composition, and it was very sensitive to the amount of $La_{0.9}Ca_{0.1}CoO_{2.95}$. The reason for this behavior is still not clear, but it is suggested that the toluene oxidation activity is strongly affected by the agglomeration state of the perovskite oxide. Actually, only 2 or 3wt% of difference in the amount of $La_{0.9}Ca_{0.1}CoO_{2.95}$ resulted in the difference of 40°C or 80°C for toluene oxidation. The most appropriate dispersion state might be obtained for the 17wt%$La_{0.9}Ca_{0.1}CoO_{2.95}$/ $Ce_{0.76}Zr_{0.19}Zn_{0.05}O_{1.95}$ catalyst, which showed the highest activity. Accordingly, the amount of La_{1-x}-$Ca_xCoO_{3-x/2}$ was adjusted to 17wt% in the present study.

Table 4.2. Complete oxidation temperature of toluene over the *y*wt%$La_{0.9}Ca_{0.1}CoO_{2.95}$/$Ce_{0.76}Zr_{0.19}Zn_{0.05}O_{1.95}$ catalysts prepared at 1400 °C.

y in $La_{0.9}Ca_{0.1}CoO_{2.95}/Ce_{0.76}Zr_{0.19}Zn_{0.05}O_{1.95}$	Complete oxidation temperature / °C
15wt%	360
17wt%	320
20wt%	400

Figure 4.3 shows XRD patterns for the 17wt%$La_{1-x}Ca_xCoO_{3-x/2}/Ce_{0.76}Zr_{0.19}Zn_{0.05}O_{1.95}$ ($0 \leq x \leq 0.15$) catalysts prepared at 1400 °C. The XRD results showed only peaks corresponding to the cubic fluorite-type oxide and perovskite-type $LaCoO_3$ structures, and no crystalline impurities were observed. The XRD peaks corresponding to the perovskite-type oxide shifted to higher angles with increasing Ca^{2+} content, but no peak shift was observed for the cubic fluorite-type oxide phase regardless of the amount of the perovskite oxide, indicating that the $La_{1-x}Ca_xCoO_{3-x/2}$ solid solutions were supported on the surface of $Ce_{0.76}Zr_{0.19}Zn_{0.05}O_{1.95}$.

The compositions of the catalysts were confirmed by the XRF analysis to be in good agreement with their stoichiometric values within the experimental errors. The BET specific surface areas of the 17wt%$La_{1-x}Ca_xCoO_{3-x/2}/Ce_{0.76}Zr_{0.19}Zn_{0.05}O_{1.95}$ catalysts are summarized in Table 4.3. They were significantly small because of the high-temperature calcination at 1400 °C. However, these catalysts showed toluene oxidation activity in spite of the small surface area. Toluene was completely oxidized into carbon dioxide and steam, and no CO or toluene-derived byproducts were detected.

Table 4.3. BET specific surface area of the 17wt%$La_{1-x}Ca_xCoO_{3-x/2}/Ce_{0.76}Zr_{0.19}Zn_{0.05}O_{1.95}$ catalysts.

x in 17wt%$La_{1-x}Ca_xCoO_{3-x/2}/Ce_{0.76}Zr_{0.19}Zn_{0.05}O_{1.95}$	BET surface area / $m^2\ g^{-1}$
0	0.9
0.03	0.4
0.07	0.3
0.10	0.5
0.12	0.3
0.15	0.4

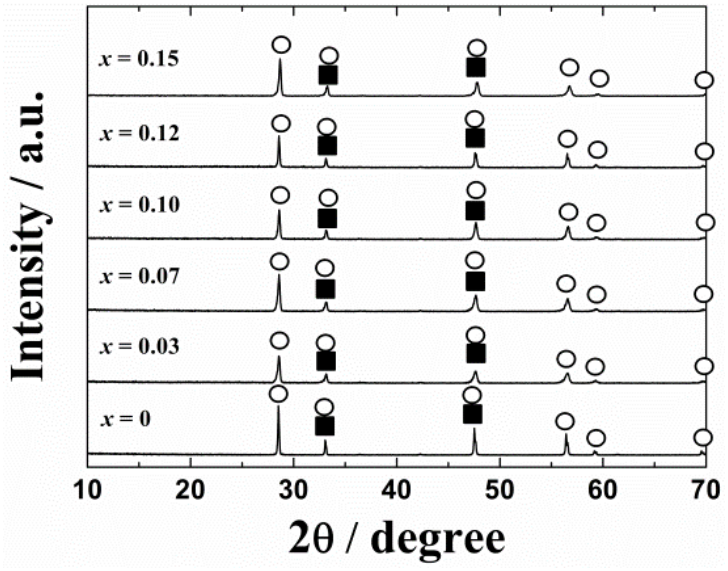

Figure 4.3. XRD patterns for 17wt%$La_{1-x}Ca_xCoO_{3-x/2}$/$Ce_{0.76}Zr_{0.19}Zn_{0.05}O_{1.95}$ catalysts. (○: $Ce_{0.76}Zr_{0.19}Zn_{0.05}O_{1.95}$; ■: $La_{1-x}Ca_xCoO_{3-x/2}$)

Figure 4.4 depicts the dependence of the complete oxidation temperature of toluene on the Ca^{2+} concentration in the 17wt%$La_{1-x}Ca_xCoO_{3-x/2}$/$Ce_{0.76}Zr_{0.19}Zn_{0.05}O_{1.95}$ ($0 \leq x \leq 0.15$) catalysts. The toluene oxidation activity depended on the catalyst composition, and the highest activity was obtained for the 17wt%$La_{0.9}Ca_{0.1}CoO_{2.95}$/$Ce_{0.76}Zr_{0.19}Zn_{0.05}O_{1.95}$ catalyst, on which the complete oxidation of toluene was realized at 320 °C.

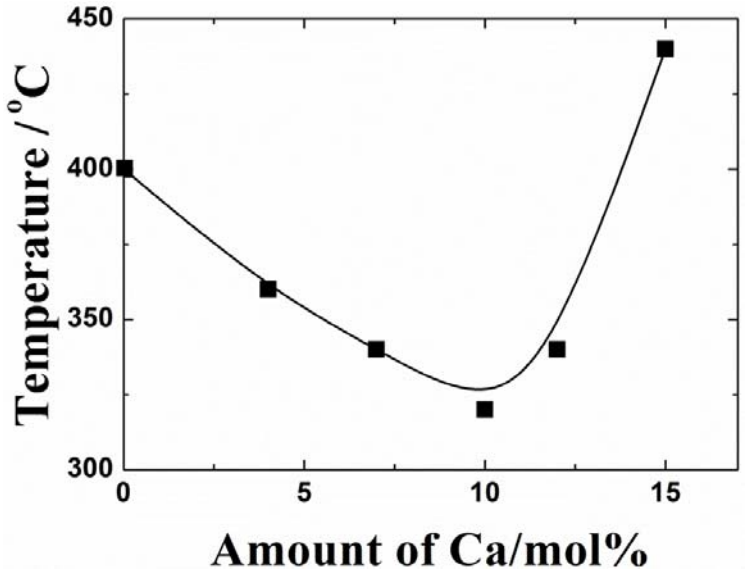

Figure 4.4. Dependence of the complete oxidation temperature of toluene on the Ca^{2+} concentration in the 17wt%$La_{1-x}Ca_xCoO_{3-x/2}$/$Ce_{0.76}Zr_{0.19}Zn_{0.05}O_{1.95}$ catalysts.

Figure 4.5 shows the XRD pattern of the 17wt%$La_{0.9}Ca_{0.1}CoO_{2.95}/Al_2O_3$ catalyst synthesized at 1400 °C. As seen in this pattern, γ-Al_2O_3 was transformed into α-Al_2O_3 and the perovskite phase was decomposed into $CoAl_2O_3$ and $LaAlO_3$. As a result, the catalytic activity of this catalyst was significantly lower than those of $La_{0.9}Ca_{0.1}CoO_{2.95}$, 17wt%$LaCoO_3/Ce_{0.76}Zr_{0.19}$-$Zn_{0.05}O_{1.95}$, and 17wt%$La_{0.9}Ca_{0.1}CoO_{2.95}/Ce_{0.76}Zr_{0.19}Zn_{0.05}O_{1.95}$ calcined at 1400 °C.

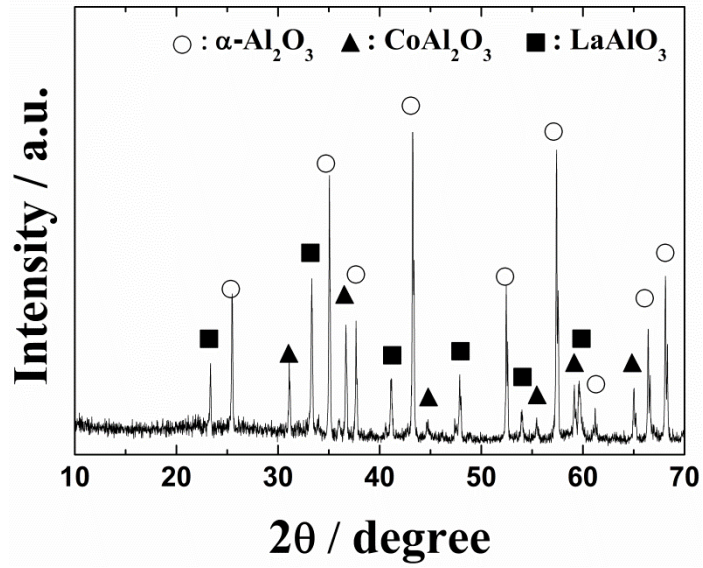

Figure 4.5. XRD pattern of the 17wt%$La_{0.9}Ca_{0.1}CoO_{2.95}/Al_2O_3$ catalyst calcined at 1400 °C.

Figure 4.6 shows the temperature dependencies of toluene oxidation over the 17wt%$LaCoO_3/Ce_{0.76}Zr_{0.19}Zn_{0.05}O_{1.95}$ and 17wt%$La_{0.9}Ca_{0.1}CoO_{2.95}/Ce_{0.76}Zr_{0.19}Zn_{0.05}O_{1.95}$ catalysts calcined at 1400 °C. For references, those of $La_{0.9}Ca_{0.1}CoO_{2.95}$ and 17wt%$La_{0.9}Ca_{0.1}CoO_{2.95}/Al_2O_3$ were also depicted. The merit of the application of the $Ce_{0.76}Zr_{0.19}Zn_{0.05}O_{1.95}$ support is evidenced by comparison with these references. The significant low activity of 17wt%$La_{0.9}Ca_{0.1}CoO_{2.95}/Al_2O_3$ was attributed to the decomposition of the perovskite phase into $CoAl_2O_3$ and $LaAlO_3$. The catalytic activity was remarkably promoted by the Ca^{2+} introduction into the $LaCoO_3$ lattice. In the case of the 17wt%$LaCoO_3/Ce_{0.76}Zr_{0.19}Zn_{0.05}O_{1.95}$ catalyst, the catalyst had to be increased 400 °C to achieve complete combustion of toluene. In contrast, toluene oxidation was completed at 320 °C through the use of the Ca-doped 17wt%$La_{0.9}Ca_{0.1}CoO_{2.95}/Ce_{0.76}Zr_{0.19}Zn_{0.05}O_{1.95}$ catalyst as mentioned above, and this temperature was lower than that observed for our conventional 0.4wt%Pt/$Ce_{0.76}$-$Zr_{0.19}Zn_{0.05}O_{1.95}$ catalyst (360 °C) calcined at 1000 °C [58]. Since the calcination temperature of the present 17wt%$La_{0.9}Ca_{0.1}CoO_{2.95}/Ce_{0.76}Zr_{0.19}Zn_{0.05}O_{1.95}$ catalyst was 1400 °C, the ΔT value corresponding to the temperature differential between complete toluene oxidation and catalyst

calcination became over 1000 °C of 1080 °C. As a result, it was elucidated that this novel catalyst can be used stably over a significantly wide temperature range. The microstructure of the 17wt%$La_{0.90}Ca_{0.10}CoO_{2.95}/Ce_{0.76}Zr_{0.19}Zn_{0.05}O_{1.95}$ catalyst was observed with a scanning electron microscope (SEM). The SEM images of 17wt%$La_{0.90}Ca_{0.10}CoO_{2.95}/Ce_{0.76}Zr_{0.19}Zn_{0.05}O_{1.95}$ catalyst are depicted in Figure 4.7. Relatively small $La_{0.90}Ca_{0.10}CoO_{2.95}$ particles about 2 μm was supported on large $Ce_{0.76}Zr_{0.19}Zn_{0.05}O_{1.95}$ support. The secondary particle size of this catalyst was smaller than 10 μm.

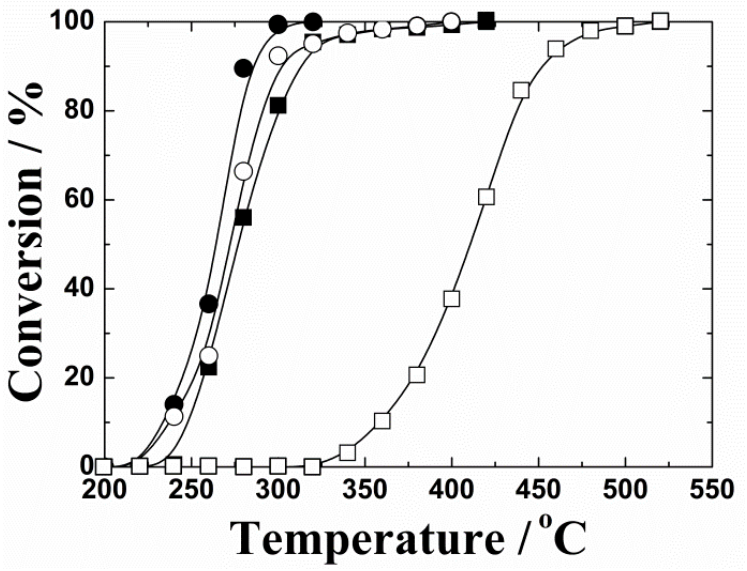

Figure 4.6. Temperature dependencies of toluene oxidation on 17wt%$La_{0.9}Ca_{0.1}CoO_{2.95}/Ce_{0.76}Zr_{0.19}$-$Zn_{0.05}O_{1.95}$ (●), 17wt%$LaCoO_3/Ce_{0.76}Zr_{0.19}Zn_{0.05}O_{1.95}$ (○), $La_{0.9}Ca_{0.1}CoO_{2.95}$ (■), and 17wt%$La_{0.9}$-$Ca_{0.1}CoO_{2.95}/Al_2O_3$ (□) catalysts calcined at 1400 °C.

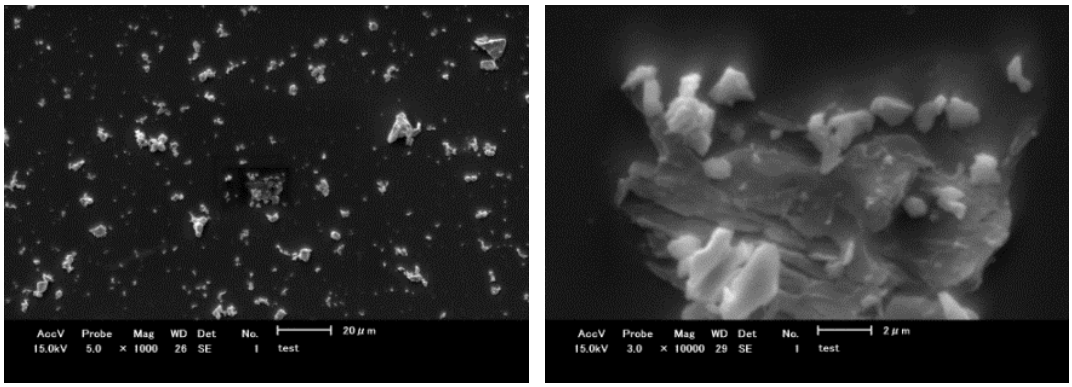

Figure 4.7. SEM images of the 17wt%$La_{0.90}Ca_{0.10}CoO_{2.95}/Ce_{0.76}Zr_{0.19}Zn_{0.05}O_{1.95}$ catalyst: (a) x1000 and (b) x10000.

The positive effect produced by the Ca^{2+} doping can be ascribed to the different reducibility of the catalysts. To evaluate this hypothesis, TPR profiles were measured for comparison of the reduction behavior of the 17wt%$LaCoO_3$/$Ce_{0.76}Zr_{0.19}Zn_{0.05}O_{1.95}$ and 17wt%$La_{0.9}Ca_{0.1}CoO_{2.95}$/$Ce_{0.76}Zr_{0.19}Zn_{0.05}O_{1.95}$ catalysts as shown in Figure 4.8. The TPR profile of 17wt%$LaCoO_3$/$Ce_{0.76}Zr_{0.19}Zn_{0.05}O_{1.95}$ (a) exhibited the first reduction peak at 350 °C. In contrast, for 17wt%$La_{0.9}Ca_{0.1}CoO_{2.95}$/$Ce_{0.76}Zr_{0.19}Zn_{0.05}O_{1.95}$ (b), oxygen release began at a lower temperature than that for 17wt%$LaCoO_3$/$Ce_{0.76}Zr_{0.19}Zn_{0.05}O_{1.95}$, and a specific reduction peak was observed at 290 °C. Each first peak in the TPR spectra corresponds to the reduction of Co^{3+} to Co^{2+} [7]. Although the peak temperatures observed in the TPR spectra were slightly higher than those of toluene oxidation, they denote the same tendency of the catalysis. Accordingly, the introduction of Ca^{2+} into the $LaCoO_3$ lattice was effective at enhancing the reducibility of the cobalt ion in the perovskite $LaCoO_3$ at lower temperatures, suggesting that the lattice oxygen released from the perovskite oxide contributes to high oxidation activity of the 17wt%$La_{0.9}Ca_{0.1}CoO_{2.95}$/ $Ce_{0.76}Zr_{0.19}Zn_{0.05}O_{1.95}$ catalyst.

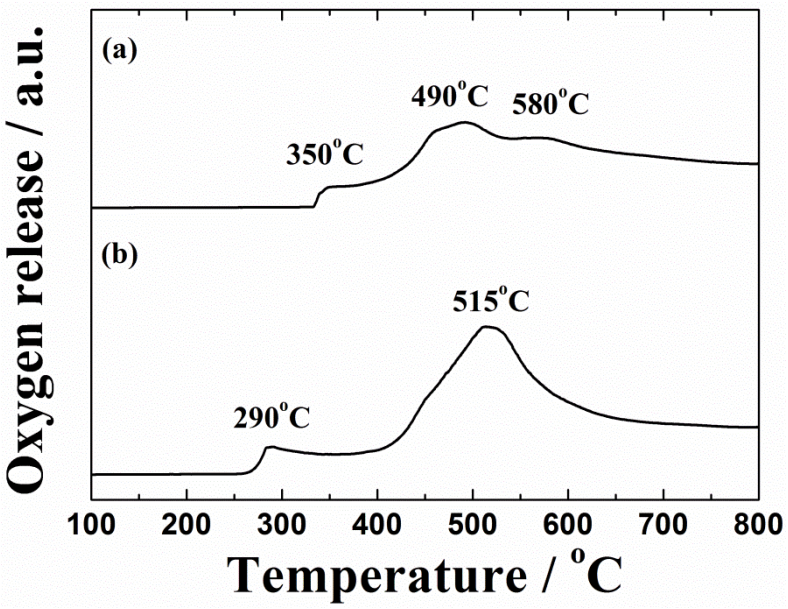

Figure 4.8. TPR profiles of a) 17wt%$LaCoO_3$/$Ce_{0.76}Zr_{0.19}Zn_{0.05}O_{1.95}$ and b) 17wt%$La_{0.9}Ca_{0.1}CoO_{2.95}$ /$Ce_{0.76}Zr_{0.19}Zn_{0.05}O_{1.95}$ catalysts calcined at 1400°C.

In addition, the OSC value of the 17wt%$La_{0.9}Ca_{0.1}CoO_{2.95}$/$Ce_{0.76}Zr_{0.19}Zn_{0.05}O_{1.95}$ catalyst was 181 μmol O_2 g^{-1}, which was 1.7 times larger than that of the 17wt%$LaCoO_3$/$Ce_{0.76}Zr_{0.19}$-$Zn_{0.05}O_{1.95}$ sample (105 μmol O_2 g^{-1}). In our previous study, we elucidated the importance of the

oxygen storage capacity (OSC) and high thermal stability of $Ce_{0.76}Zr_{0.19}Zn_{0.05}O_{1.95}$ to facilitate toluene oxidation even after calcination at high temperatures [10]. These properties actually effective to enhance the catalytic activity of the $La_{0.9}Ca_{0.1}CoO_{2.95}$ catalyst, as already evidenced in Figure 4.5 by the comparison with the activities of $La_{0.9}Ca_{0.1}CoO_{2.95}$ without the $Ce_{0.76}Zr_{0.19}Zn_{0.05}O_{1.95}$ support and 17wt%$La_{0.9}Ca_{0.1}CoO_{2.95}/Al_2O_3$.

4.4. Conclusions

The novel 17wt%$La_{1-x}Ca_xCoO_{3-x/2}/Ce_{0.76}Zr_{0.19}Zn_{0.05}O_{1.95}$ ($0 \leq x \leq 0.15$) catalysts were synthesized at 1400 °C to realize refractory and noble metal-free materials. The complete oxidation of toluene was realized at a temperature of 320 °C using the 17wt%$La_{0.9}Ca_{0.1}CoO_{2.95}$/ $Ce_{0.76}Zr_{0.19}Zn_{0.05}O_{1.95}$ catalyst prepared at 1400 °C. Therefore, catalytic tests for toluene oxidation and characterization of oxygen release/storage properties on these materials confirmed that the Ca^{2+} doping into the $LaCoO_3$ lattice was significantly effective in facilitating toluene oxidation even after high-temperature calcination at 1400 °C. As a result, the ΔT value corresponding to the temperature differential between complete toluene oxidation and catalyst calcination became 1080 °C, clarifying that this catalyst can work even after being exposed to significantly high temperatures by the combustion heat. Furthermore, $La_{0.9}Ca_{0.1}CoO_{2.95}$ on the $Ce_{0.76}Zr_{0.19}Zn_{0.05}O_{1.95}$ support promoted toluene oxidation without using the expensive and precious platinum metal, and, therefore, this catalyst has reasonable potential as a novel toluene oxidation catalyst.

Summary

In the study of this thesis, the development of novel catalysts that can be realized high thermal stability and complete oxidation of toluene at moderate heating temperatures without the formation of any toluene combustion by-products. To be more specific developed the catalyst for complete combustion of toluene at as low a temperature as possible, researched to decrease in the amount of contained platinum, or to avoid the use of platinum. Furthermore, the catalyst have realized to the excellent thermal stability and complete combustion of toluene for continued activation that exposed to the heat of combustion for over 1000 ^{o}C. In addition, novel material possessing excellent oxygen storage and release abilities was also developed to facilitate complete oxidation.

The results obtained through this work are summarized as follows:

Chapter 1

The novel Co_3O_4/CeO_2-ZrO_2-SnO_2/γ-Al_2O_3 and $Pt/Co_3O_4/CeO_2$-ZrO_2-SnO_2/γ-Al_2O_3 catalysts were successfully developed to realize complete oxidation of toluene into carbon dioxide and steam at moderate heating temperature. In order to design active and stable oxidation catalysts, active oxygen supplied from the CeO_2-ZrO_2-SnO_2 support was combined with high oxidation activity of Co_3O_4 and Pt catalyst. The catalytic tests for toluene oxidation on these materials showed that addition of Co_3O_4 to a Pt/CeO_2-ZrO_2-SnO_2/γ-Al_2O_3 catalyst was significantly effective in decreasing the amount of platinum without significant reduction in the activity. As a result, complete oxidation of toluene was realized using the 1wt%Pt/11wt%Co_3O_4/16wt%$Ce_{0.62}Zr_{0.20}$-$Sn_{0.18}O_{2.0}/\gamma$-Al_2O_3 catalyst at 160 °C without the formation of toluene combustion by-products, which was lower than that using the 5wt%Pt/γ-Al_2O_3 catalyst (170 °C). Since the oxidation activities of 1wt%Pt/16wt%$Ce_{0.62}Zr_{0.20}Sn_{0.18}O_{2.00}/\gamma$-$Al_2O_3$ and 1wt%Pt/11wt%Co_3O_4/γ-Al_2O_3 were lower than that of 1wt%Pt/11wt%Co_3O_4/16wt%$Ce_{0.62}Zr_{0.20}Sn_{0.18}O_{2.00}/\gamma$-$Al_2O_3$, the cause for the high toluene oxidation activity observed in the 1wt%Pt/11wt%Co_3O_4/16wt%$Ce_{0.62}Zr_{0.20}Sn_{0.18}O_{2.00}$ $/\gamma$-Al_2O_3 catalyst can be attributed to the concerted effect of Pt, Co_3O_4, and $Ce_{0.62}Zr_{0.20}Sn_{0.18}O_{2.00}$ supported on γ-Al_2O_3.

Chapter 2

Complete oxidation of toluene was investigated on the concerted effect of Co_3O_4 and CeO_2-ZrO_2-SnO_2 support. The catalytic activities for toluene were remarkably increased by the active oxygen supply ability. Therefore, used to the varied supports, the complete oxidation of toluene was realized using the 16.9wt%Co_3O_4/$Ce_{0.67}Zr_{0.18}Sn_{0.15}O_{2.00}$ catalyst at a temperature of 260 °C, which was lower than those for 16.8wt%Co_3O_4/$Ce_{0.78}Zr_{0.22}O_{2.00}$ (300 °C) and 16.8wt%Co_3O_4/$Ce_{0.64}Zr_{0.15}Bi_{0.21}O_{1.895}$ (280 °C).

The novel Co_3O_4/CeO_2-ZrO_2-SnO_2 catalysts were successfully prepared by the evaporative drying method and the composition was optimized to give the highest toluene oxidation activity. Catalytic tests for toluene oxidation and characterization of oxygen release/storage properties on these materials showed that the readily reducible property of the CeO_2-ZrO_2-SnO_2 support was significantly effective in facilitating toluene oxidation. Furthermore, the toluene oxidation activity was maintained even in the presence of moisture. Since Co_3O_4 on the CeO_2-ZrO_2-SnO_2 supports promoted the toluene oxidation without using the expensive and precious platinum metal, the 16.9wt%Co_3O_4/$Ce_{0.67}Zr_{0.18}Sn_{0.15}O_{2.00}$ catalyst has the potential as a novel environmental catalyst for toluene cleaning at moderate temperatures.

Chapter 3

The novel Pt/CeO_2-ZrO_2-ZnO catalysts were successfully developed to realize complete oxidation of toluene into carbon dioxide, steam and toluene combustion by-products. Catalytic tests for toluene oxidation and characterization of oxygen release/storage properties on catalyst showed that the thermal stability of the CeO_2-ZrO_2-ZnO support was significantly effective in facilitating toluene oxidation even after high-temperature calcination at 1000 °C. In addition, the catalytic test up to 1000 °C was repeated three times to evaluate thermal stability of the 0.4wt%Pt/$Ce_{0.76}Zr_{0.19}$-$Zn_{0.05}O_{1.95}$ catalyst. Moreover, the complete oxidation of toluene was realized at a temperature of 360 °C, where the temperature was lower than that for 0.4wt%Pt/$Ce_{0.73}Zr_{0.21}Sn_{0.06}O_{2.0}$ (460 °C) calcined at 1000 °C. Furthermore, the toluene oxidation activity was maintained even in the presence of moisture.

Chapter 4

The novel refractory and noble metal-free 17wt%$La_{1-x}Ca_xCoO_{3-x/2}$/$Ce_{0.76}Zr_{0.19}Zn_{0.05}O_{1.95}$ ($0 \leq x \leq 0.15$) catalysts were prepared for complete toluene oxidation and the composition was optimized to give the highest toluene oxidation activity. Catalytic tests for toluene oxidation and characterization of oxygen release/storage properties on these materials showed that the Ca^{2+} doping into the $LaCoO_3$ lattice was significantly effective in facilitating toluene oxidation even after high-temperature calcination at 1400 °C. On this catalyst, the composition and the complete oxidation of toluene were optimized to give the highest toluene oxidation activity. Furthermore, temperature differential between complete toluene oxidation and catalyst calcination on this catalyst was over 1000 °C, elucidating that this novel catalyst can be used stably over a significantly wide temperature range. In fact, complete oxidation of toluene was realized at a temperature of 320 °C using the 17wt%$La_{0.9}Ca_{0.1}CoO_{2.95}$/$Ce_{0.76}Zr_{0.19}Zn_{0.05}O_{1.95}$ catalyst prepared at 1400 °C. As a result, the ΔT value corresponding to the temperature differential between complete toluene oxidation and catalyst calcination became 1080 °C, clarifying that this catalyst can work even after being exposed to significantly high temperatures by the combustion heat. Furthermore, $La_{0.9}Ca_{0.1}CoO_{2.95}$ on the $Ce_{0.76}Zr_{0.19}Zn_{0.05}O_{1.95}$ support promoted toluene oxidation without using the expensive and precious platinum metal, and, therefore, this catalyst has reasonable potential as a novel toluene oxidation catalyst.

References

[1] R. Atkinson, J. Arey, *Chem. Rev.*, **103**, 4605-4638 (2003).

[2] T.B. Ryerson, M. Trainer, J.S. Holloway, D.D. Parrish, L.G. Huey, D.T. Sueper, G.J. Frost, S.G. Donnelly, S. Schauffler, E.L. Atlas, W.C. Kuster, P.D. Goldan, G. Hübler, J.F. Meagher, F.C. Fehsenfled, *Science*, **292**, 719-723 (2001).

[3] I.E. Sungkono, H.Kameyama, T. Koya, *Appl. Surf. Sci.*, **121/122**, 425-428 (1997).

[4] A. Hamins, K. Seshadri, *Combust. Flame.*, **68**, 295-307 (1987).

[5] A.M. Harling, D.J. Glover, J.C. Whitehead, K. Zhang, *Appl. Catal. B: Environ.*, **90**, 157-161 (2009).

[6] H. Einaga, S. Futamura, T. Ibusuki, *Appl. Catal. B: Environ.*, **38**, 215-225 (2002).

[7] F. Hauxell, R.H. Ottewill, *J. Colloid. Interface. Sci.*, **28**, 514-521 (1968).

[8] J.J. Spivey, *Ind. Eng. Chem. Res.*, **26**, 2165-2180 (1987).

[9] S.M. Saqer, D.I. Kondarides, X.E. Verykios, *Top. Catal.*, **52**, 517-527 (2009).

[10] N. Imanaka, T. Masui, K. Yasuda, *Chem. Lett.*, **40**, 780-785 (2011).

[11] A.C. Gluhoi, B.E. Nieuwenhuys, *Catal. Today*, **119**, 305-310 (2007).

[12] S.C. Kim, *J. Hazard. Mater.*, **91**, 285-299 (2002).

[13] Y. Li, X. Zhang, H. He, Y. Yu, T. Yuan, Z. Tian, J. Wang, Y. Li, *Appl. Catal. B*, **89**, 659-664 (2009).

[14] J. Chi-Sheng Wu, T.Y. Chang, *Catal. Today*, **44**, 111-118 (1998).

[15] S. Ojala, Catalytic oxidation of volatile organic compounds and malodorous organic compounds. Ph. D. Thesis, University of Oulu, Finland, pp. 15-27 (2005).

[16] P. Papaefthimiou, T. Ioannides, X.E. Verykios, *Appl. Catal. B*, **13**, 175-184 (1997).

[17] W. Shen, X. Dong, Y. Zhu, H. Chen, J. Shi, *Micropor. Mesopor. Mat.*, **85**, 157-162 (2005).

[18] J. Hermia, S. Vigneron, *Catal. Today*, **17**, 349-358 (1993).

[19] A. O´Malley, B.K. Hodnett, *Catal. Today*, **54**, 31-38 (1999).

[20] S. M. Saqer, D.I. Kondarides, X.E. Verykios, *Top. Catal.*, **52**, 517-527 (2009).

[21] M.A. Alvarez-Merino, M.F. Ribeiro, J.M. Silva, F. Carrasco-Marín, F.J. Maldonado-Hódar, *Environ. Sci. Technol.*, **38**, 4664-4670 (2004).

[22] N.M. Rodriguez, S.G. Oh, R.A. Dalla-Betta, R.T.K. Baker, *J. Catal.*, **157**, 676-686 (1995).

[23] H. Arai, H. Fukuzawa, *Catal. Today*, **26**, 217-221 (1995).

[24] H.L. Liu, H. Ma, S. Shao, Z. Li, A. Wang, Y. Huang, T. Zhang, *Chin. J. Catal.*, **28**, 1077-1082 (2007).

[25] A. Parinyaswan, S. Pongstabodee, A. Luengnaruemitchai, *Int. J. Hydrogen Energy*, **31**, 1942-1949 (2006).

[26] S. Damyanova, J.M.C. Bueno, *Appl. Catal. A*, **253**, 135-150 (2003).

[27] K. Yasuda, T. Masui, N. Imanaka, *Funct. Mater. Lett.*, **4**, 411-414 (2011).

[28] N. Imanaka, T. Masui, *Chem. Rec.*, **9**, 40-50 (2009).

[29] T. Masui, H. Imadzu, N. Mastuyama, N. Imanaka, *J. Hazard. Mater.*, **176**, 1106-1109 (2010).

[30] K. Yasuda, M. Nobu, T. Masui, N. Imanaka, *Mater. Res. Bull.*, **45**, 1278-1282 (2010).

[31] K. Yasuda, A. Yoshimura, A. Katsuma, T. Masui, N. Imanaka, *Bull. Chem. Soc. Jpn.*, **85**, 522-526 (2012).

[32] M. Batzill, U. Diebold, *Prog. Surf. Sci.*, **79**, 47-154 (2005).

[33] A. Janotti, C. G. Van de Walle, *Rep. Prog. Phys.*, **72**, 126501 (2009).

[34] N. Imanaka, T. Masui, K. Minami, K. Koyabu, *Chem. Mater.*, **17**, 6511-6513 (2005).

[35] K. Minami, T. Masui, N. Imanaka, L. Dai, B. Pacaud, *J. Alloys. Compd.*, **408-412**, 1132-1135 (2006).

[36] N. Imanaka, T. Masui, K. Koyabu, K. Minami, T. Egawa, *Adv. Mater.*, **19**, 1608-1611 (2007).

[37] T. Masui, K. Koyabu, K. Minami, T. Egawa, N. Imanaka, *J. Phys. Chem. C*, **111**, 13892-13897 (2007).

[38] T. Masui, K. Minami, K. Koyabu, N. Imanaka, *Catal. Today*, **117**, 187-192 (2006).

[39] N. Imanaka, T. Masui, A. Terada, H. Imadzu, *Chem. Lett.*, **37**, 42-43 (2008).

[40] J.F. Lamonier, A.B. Boutoundou, C. Gennequin, M.J. Perez-Zurita, S. Siffert, A. Aboukais, *Catal. Lett.*, **118**, 165-172 (2007).

[41] F. Wyrwalski, J.M. Giraudon, J.F. Lamonier, *Catal. Lett.*, **137**, 141-149 (2010).

[42] P. Rybak, B. Tomaszewska, A. Machocki, W. Grzegorczyk, A. Denis, Catal. Today, **176**, 14-20 (2011).

[43] R.R. Chianelli, G. Berhault, B. Torres, *Catal. Today*, **147**, 275-286 (2009).

[44] L.F. Liotta, M. Ousmane, G.D. Carlo, G. Pantaleo, G. Deganello, A. Boreave, A.G. Fendler, *Catal. Lett.*, **127**, 270-276 (2009).

[45] A.M.G. Pedrosa, M.J.B. Souza, J.D.G. Fernandes, D.M.A. Melo, A.S. Araujo, *React. Kinet. Catal. Lett.*, **79**, 391-396 (2003).

[46] L.F. Liotta, G. Di Carlo, G. Pantaleo, A.M. Venezia, G. Danello, *Appl. Catal. B: Environ.*, **66**, 217-227 (2006).

[47] E. Beche, P. Charvin, D. Perarnau, S. Abanades, G. Flamant, *Surf. Interf. Anal.*, **40**, 264-267 (2008).

[48] Y. Ma, Q. Ge, W. Li, and H. Xu, *Appl. Catal. B: Environ.*, **90**, 99-104 (2009).

[49] L. Kover, Zs. Kovacs, R. Sanjines, G. Mretti, I. Cserny, G. Margaritondo, *J. Palinkas, and H. Adachi, Surf. Interf. Anal.*, **23**, 461-466 (1995).

[50] Q. Xiao, J. Zhang, C. Xiao, X. Tan, *Catal. Commun.***, 9**, 1247-1253 (2008).

[51] X. Zhang, K. Chan, *Chem. Mater.*, **15**, 451-459 (2003).

[52] R.D. Shannon, *Acta Cryst.*, **A32**, 751-767 (1976).

[53] T.B. Nguyen, J.P. Deloume, V. Perrichon, *Appl. Catal. A : Gen.*, **249**, 273-284 (2003).

[54] Q. Dong, S. Yin, C. Guo, T. Sato, *Catal. Sci. Technol.*, **2**, 2521-2524 (2012).

[55] T. Baidya, A. Gupta, P.A. Deshpandey, G. Madras, M.S. Hegde, *J. Phys. Chem. C*, **113**, 4059-4068 (2009).

[56] M. Y. Kim, T. Kamata, T. Masui, N. Imanaka, *J. Mater. Sci. Res.*, **2**, 51-59 (2013).

[57] M. Y. Kim, T. Kamata, T. Masui, N. Imanaka, *J. Asian Ceram. Soc.*, **1**, 243-247 (2013).

[58] M. Y. Kim, T. Kamata, T. Masui, N. Imanaka, *Catalysts*, **3**, 646-655 (2013).

[59] A. Janotti, C. G. Van de Walle, *Phys. Rev. B*, **76**, 165202 (2007).

[60] H. Tanaka, I. Tan, M. Uenishi, M. Kimura, K. Dohmae, *Top. Catal.*, **16-17**, 63-70 (2001).

[61] Y. Nishihata, J. Mizuki, T. Akao, H. Tanaka, M. Uenishi, M. Kimura, T. Okamoto, N. Hamada, *Nature*, **418**, 164-167 (2002).

[62] S. Yamaguchi, Y. Okimoto, Y. Tokura, *Phys. Rev. B.*, **54**, R11022-R11025 (1996).

[63] R. Pereñíguez, J. L. Hueso, F. Gaillard, J. P. Holgado, A. Caballero, *Catal. Lett.*, **142**, 408-416 (2012).

Acknowledgments

The author would like to express his heartfelt gratitude to Professor Dr. Nobuhito Imanaka, Department of Applied Chemistry, Graduate School of Engineering, Osaka University, for his continuous guidance, his invaluable suggestions, and his science encouragement throughout the work. The author is very grateful to Professor Dr. Toshiyuki Masui, Department of Applied Chemistry, Graduate School of Engineering, Osaka University, for his continuous guidance and stimulating discussions for carrying out this work. The author is also indebted to Dr. Shinji Tamura, Department of Applied Chemistry, Graduate School of Engineering, Osaka University, for his helpful suggestions and heartfelt advice.

The author is deeply grateful to Professor Dr. Susumu Kuwabata, Department of Applied Chemistry, Graduate School of Engineering, Osaka University, and Professor Dr. Yoichi Ando, The institute of Scientific and Industrial Research (Department of Applied Chemistry, Graduate School of Engineering), Osaka University, for reviewing this thesis and giving their valuable comments.

Special thanks should be given to author's co-workers, Dr. Keisuke Yasuda, Dr. Naoyoshi Nunotani, Mr. Wendusu, Mr. Kazuya Jyoko, Mr. Atsushi Katsuma, Mr. Tomoya Kamata, Mr. Fukuhara Nashito, Mr. Shunji Uejima, Mr. Takanobu Ono, Mr. Taihei Honda, Mr. Soichiro Tsujimoto, and Dr. Sun Woog Kim for their helpful assistance and support in the course of this work, and members of the research group under direction of Professor Dr. Nobuhito Imanaka, Osaka University.

The Yoshida Scholarship 'Asia 100' had to support for a life of studying abroad in Japan and my family would like to thank Yoshida Scholarship Foundation for their support.

The author would like to thank to Professor Dr. Dong Sik Bae of Changwon National University in South Korea for his helpful comments and encouragement.

Finally, the author would like to deeply thank to his parents Mr. Il Sik Kim and Mrs. Kyoung Hee Kim, and my sister Ms. Ga Lyeom Jeong Kim, and all the members of his family for their encouragement, continuous understanding, and perpetual supports.